

## STRONG EVIDENCE FOR GAMMA-RAY LINE EMISSION FROM THE INNER GALAXY

MENG SU<sup>1,3</sup>, DOUGLAS P. FINKBEINER<sup>1,2</sup>

*Draft version October 29, 2018*

### ABSTRACT

Using 3.7 years of *Fermi*-LAT data, we examine the diffuse 80 – 200 GeV emission in the inner Galaxy and find a resolved gamma-ray feature at  $\sim 110 - 140$  GeV. We model the spatial distribution of this emission with a  $\sim 3^\circ$  FWHM Gaussian, finding a best fit position  $1.5^\circ$  West of the Galactic Center. Even better fits are obtained for off-center Einasto and power-law profiles, which are preferred over the null (no line) hypothesis by  $6.5\sigma$  ( $5.0\sigma/5.4\sigma$  after trials factor correction for one/two line case) assuming an NFW density profile centered at  $(\ell, b) = (-1.5^\circ, 0^\circ)$  with a power index  $\alpha = 1.2$ . The energy spectrum of this structure is consistent with a single spectral line (at energy  $127.0 \pm 2.0$  GeV with  $\chi^2 = 4.48$  for 4 d.o.f.). A pair of lines at  $110.8 \pm 4.4$  GeV and  $128.8 \pm 2.7$  GeV provides a marginally better fit (with  $\chi^2 = 1.25$  for 2 d.o.f.). The total luminosity of the structure is  $(3.2 \pm 0.6) \times 10^{35}$  erg/s, or  $(1.7 \pm 0.4) \times 10^{36}$  photons/sec. The energies in the two-line case are compatible with a  $127.3 \pm 2.7$  GeV WIMP annihilating through  $\gamma\gamma$  and  $\gamma Z$  (with  $\chi^2 = 1.67$  for 3 d.o.f.). We describe a possible change to the *Fermi* scan strategy that would accumulate S/N on spectral lines in the Galactic center 4 times as fast as the current survey strategy.

*Subject headings:* gamma rays — diffuse emission — milky way — dark matter

### 1. INTRODUCTION

Although various cosmological and astrophysical observations provide compelling evidence for dark matter (DM), which constitutes  $\sim 80\%$  of the matter in the Universe, we still know little about its intriguing nature (e.g. Bertone et al. 2005; Hooper & Profumo 2007). Among a forest of dark matter models, stable Weakly Interacting Massive Particles (WIMP) have been predicted in many extensions of the Standard Model of particle physics (e.g. Bergström 2000). The WIMP with the virtues of weak scale masses and couplings is an excellent dark matter particle candidate which can annihilate into high energy gamma-rays (e.g. Bergström et al. 1998). The inner Galaxy provides one of the most promising regions on the sky to search for WIMP annihilation produced gamma rays (Ackermann et al. 2011; Abramowski et al. 2011; Gondolo & Silk 1999). The expected relatively higher annihilation rate due to higher dark matter particle density provides a potential window to identify any non-gravitational dark matter signatures.

The “smoking-gun” signal of annihilating dark matter would be a monochromatic gamma-ray line (or lines) in a region of high dark matter density, either in local dwarf galaxies or in the Galactic center. This line could be produced by dark matter decays or annihilations into two photons, or two-body final states involv-

ing one photon plus a Higgs boson, Z boson, or other chargeless non-SM particle. In most models, dark matter does not annihilate directly to photons, but in models where it annihilates to charged lepton pairs, there may be loop interactions that produce photons in two-body final states, yielding spectral lines. These lines can provide a signature of dark matter even in a complicated astrophysical environment, because no known astrophysical process produces gamma-ray lines at  $E \gg 1$  GeV. However, these loop processes would be suppressed by 1-4 orders of magnitude compared to the total annihilation or decay rate (e.g. Bergström & Ullio 1997). The unprecedented sensitivity and spectral resolution of the Large Area Telescope (LAT; Gehrels & Michelson 1999; Atwood et al. 2009) aboard the *Fermi Gamma-ray Space Telescope* make it possible to search for dark matter annihilation lines over the whole sky up to a few hundred GeV.

However, other signals can mimic a weak line. Features such as a spectral edge or a broken power law can be mistaken for a line in noisy data, especially when smoothed by the instrumental response. Thus careful separation of possibly diffuse dark matter emission from other diffuse components is crucial.

For example, the *Fermi* bubbles extend  $\sim 10$  kpc above and below the Galactic center (GC) (Su et al. 2010). Their emission has a flat energy spectrum in  $E^2 dN/dE$  from hundreds of MeV to  $\sim 100$  GeV implying the ability of the *Fermi* bubbles to accelerate cosmic ray (CR) electrons up to  $\sim$ TeV, if the gamma rays are produced by inverse Compton (IC) scattering of the Cosmic Microwave Background (CMB) photons (Su et al. 2010).

<sup>1</sup> Institute for Theory and Computation, Harvard-Smithsonian Center for Astrophysics, 60 Garden Street, MS-51, Cambridge, MA 02138 USA

<sup>2</sup> Physics Department, Harvard University, Cambridge, MA 02138 USA

<sup>3</sup> mengsu@cfa.harvard.edu

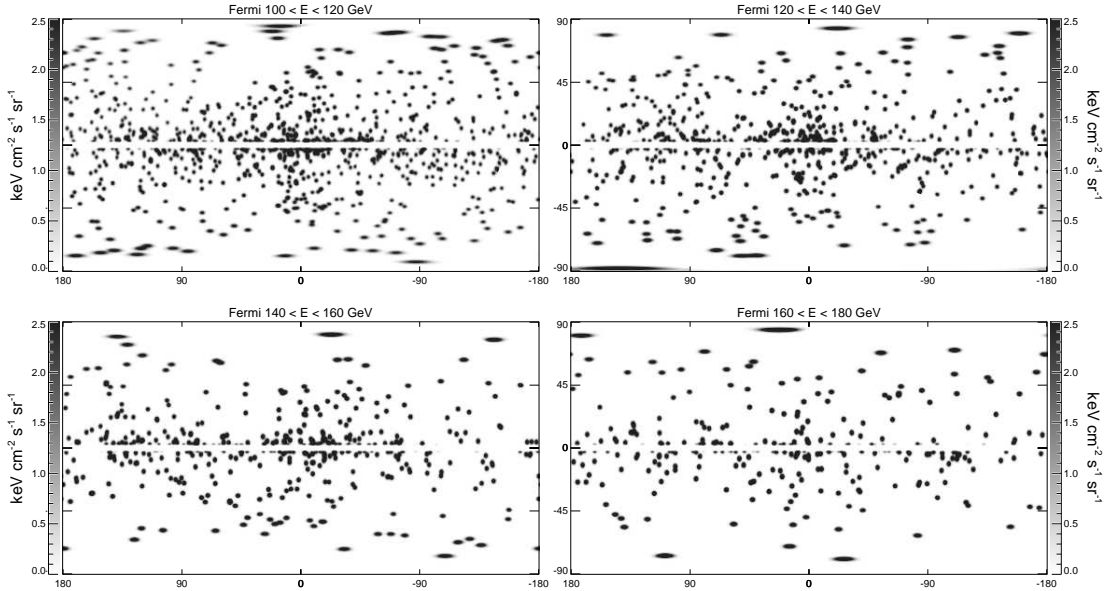


FIG. 1.— All-sky *Fermi*-LAT 3.7 year sky maps in 4 energy bins ranging from 100 to 180 GeV. We use CLEAN event class and point sources have been subtracted based on the Second *Fermi*-LAT catalog (2FGL). Large sources, including the inner disk ( $-2^\circ < b < 2^\circ$ ,  $-180^\circ < \ell < 180^\circ$ ), have been masked. The maps have been smoothed for display with a Gaussian kernel of FWHM =  $2^\circ$ .

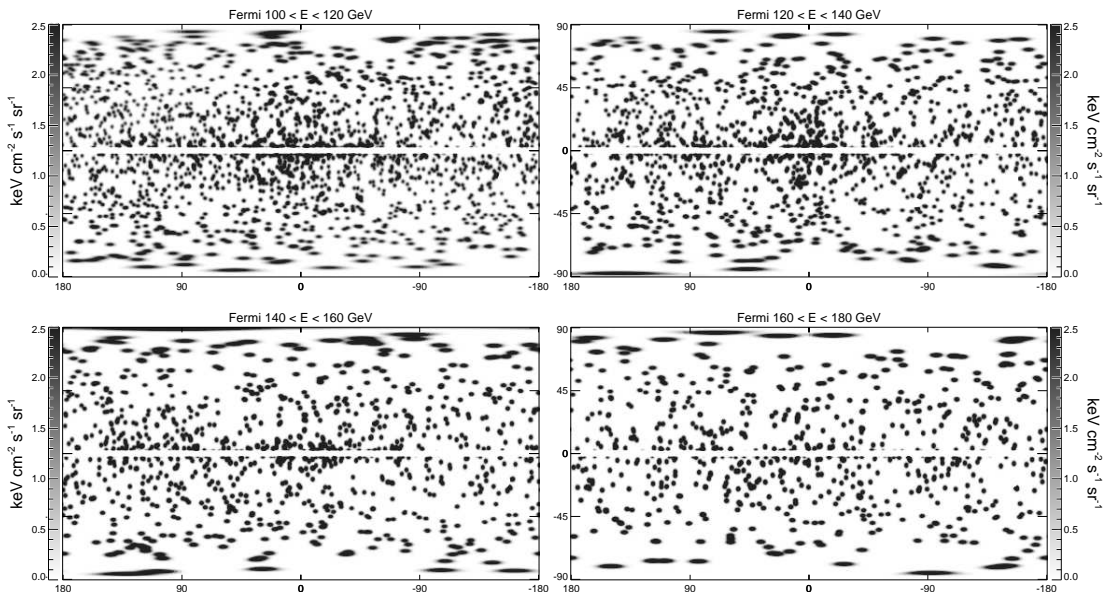


FIG. 2.— Same as Figure 1, but with SOURCE class events. This event class contains substantially more background.

If there is a spectral break in the *Fermi* bubble spectrum at high energy, the superposition of such a spectrum with other soft-spectrum diffuse components might mimic a bump feature on top of a continuum power law (Profumo & Linden 2012).

In this work, we use 3.7 years data of LAT to study the diffuse gamma-ray emission toward the inner Galaxy at  $80 < E_\gamma < 200$  GeV. In Section 2 we describe our LAT data selection and map making. In Section 3, we show that the gamma-ray maps reveal a novel gamma-ray cusp toward the Galactic center. We characterize the

morphology of the gamma-ray cusp and employ regression template fitting to determine its energy spectrum in Section 4. In Section 5 we study the detailed spatial profile of the cusp structure by fitting various templates. Section 6 contains analysis of the spectral line profile, and searches for instrumental effects in photon samples from the Galactic plane and the Earth's limb. We derive the energy spectrum of the cusp assuming various dark matter density profiles in Section 7. We propose a modified survey strategy in Section 8 that would allow *Fermi*-LAT to confirm this gamma-ray line signal in  $\sim 1$

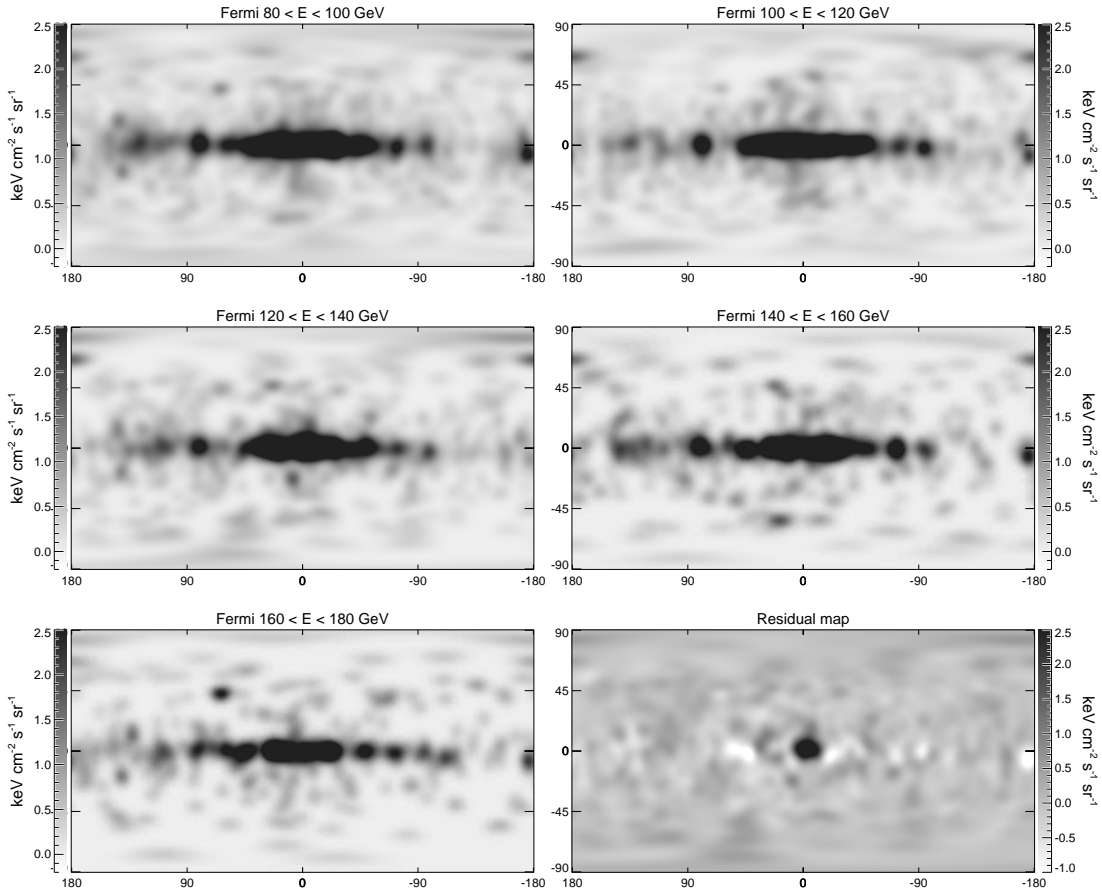


FIG. 3.— All-sky CLEAN 3.7 year maps in 5 energy bins, and a residual map (*lower right*). The residual map is the 120 – 140 GeV map minus a background estimate, taken to be the average of the other 4 maps where the average is computed in  $E^2 dN/dE$  units. This simple background estimate is sufficient to remove the Galactic plane and most of the large-scale diffuse structures and even bright point sources. A cuspy structure toward the Galactic center is revealed as the only significant structure in the residual gamma-ray map. All of the maps are smoothed with a Gaussian kernel of  $\text{FWHM} = 10^\circ$  without source subtraction.

year with no trials factor, and we summarize our main findings in Section 9.

## 2. MAP CONSTRUCTION

For this project, we constructed full-sky maps from the LAT event files as in our previous work (Dobler et al. 2010; Su et al. 2010; Su & Finkbeiner 2012), except that we now use 3.7 years of Pass 7 (P7\_V6) data.

### 2.1. Fermi data selection

The *Fermi* LAT is a pair-conversion telescope, in which incoming photons convert to  $e^+e^-$  pairs, which are then tracked through the detector. The arrival direction and energy of each event are reconstructed, and the time of arrival recorded. Event files for every week of the mission are available on the Internet, and it is from these files that we build our maps.

The point spread function (PSF) is about  $0.8^\circ$  for 68% containment at 1 GeV and decreases with energy as  $r_{68} \sim E^{-0.8}$ , asymptoting to  $\sim 0.2^\circ$  at high energy. The LAT is designed to survey the gamma-ray sky in the energy range from about 20 MeV to several hundreds of GeV.

We use the latest publicly available data and instru-

ment response functions, known as Pass 7 (P7\_V6)<sup>4</sup>. For most figures in this work we use the CLEAN event class, which has larger effective area than ULTRACLEAN and lower background than SOURCE. In a few cases, we show figures made with ULTRACLEAN or SOURCE events as evidence that this choice has no qualitative effect on our results.

Photons coming from the bright limb at Earth’s horizon, dominantly produced by grazing-incidence CR showers in the atmosphere, are a potential source of contamination. We minimize this background by selecting events with zenith angle less than  $100^\circ$  as suggested in the *Fermi* Cicerone<sup>5</sup>. We also exclude some time intervals, primarily while *Fermi* passes through the South Atlantic Anomaly.

### 2.2. Map making

We generate full-sky maps of counts and exposure using HEALPix, a convenient equal-area iso-latitude full-

<sup>4</sup> Details at [http://fermi.gsfc.nasa.gov/ssc/data/analysis/documentation/Pass7\\_usage.html](http://fermi.gsfc.nasa.gov/ssc/data/analysis/documentation/Pass7_usage.html)

<sup>5</sup> <http://fermi.gsfc.nasa.gov/ssc/data/analysis/documentation/>.

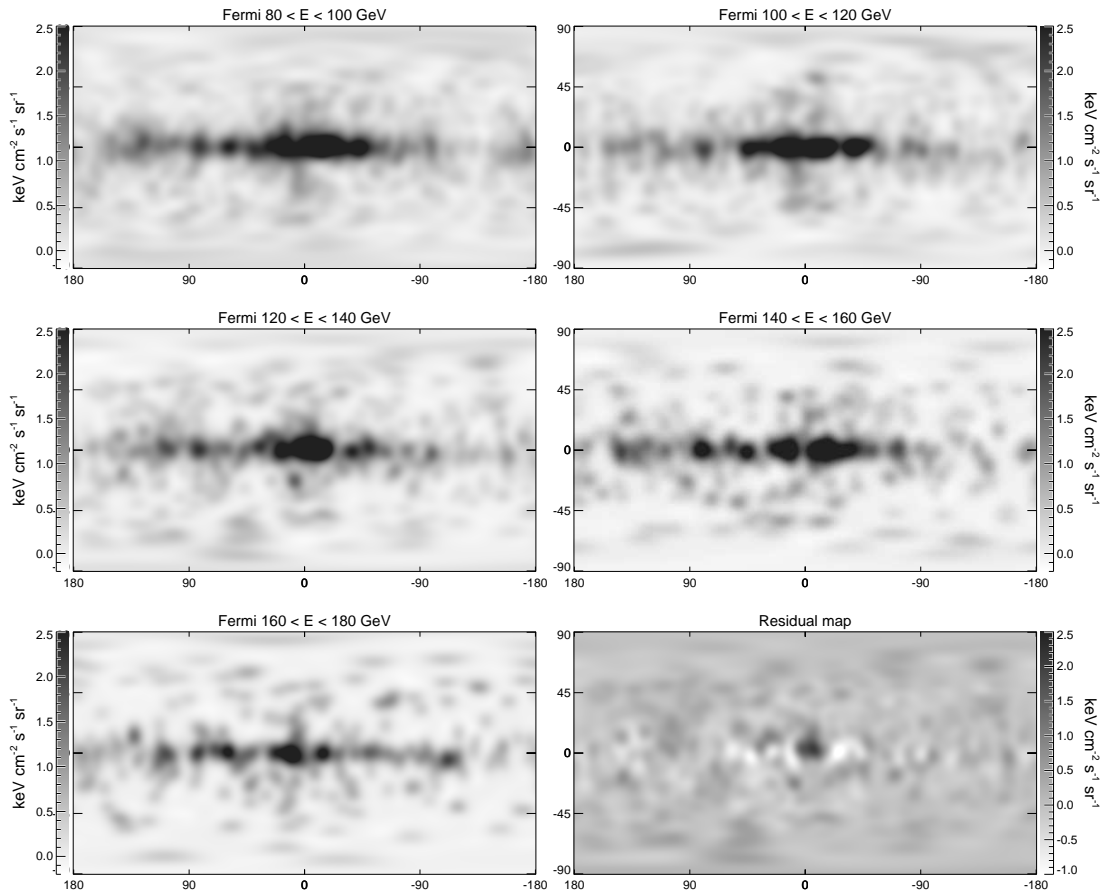


FIG. 4.— The same as Figure 3 but we have subtracted point sources before smooth the maps.

sky pixelization widely used in the CMB community.<sup>6</sup> Spherical harmonic smoothing is straightforward in this pixelization, and we smooth each map by the kernel required to obtain an approximately Gaussian PSF of some target FWHM, usually  $10^\circ$ . We generate maps for front- and back-converting events separately, smooth them to a common PSF, and then combine them.

We construct maps both with and without point source subtraction. We subtract point sources listed in the Second *Fermi*-LAT catalog (2FGL), which is based on 24 months of P7\_V6 LAT observations.<sup>7</sup> The PSF and effective area of the *Fermi*-LAT varies with energy, and we subtract each point source from the maps in each energy bin, using the in-flight version of the PSF contained in the P7\_V6 IRFs.

For the 400 brightest and 400 most variable sources, the subtraction is noticeably imperfect at lower energies (and we assume it is also at the higher energies used in this work), so we interpolate over the core of the PSF

<sup>6</sup> HEALPix software and documentation can be found at <http://healpix.jpl.nasa.gov>, and the IDL routines used in this analysis are available as part of the IDLUTILS product at <http://sdss3data.lbl.gov/software/idlutils>.

<sup>7</sup> [http://fermi.gsfc.nasa.gov/ssc/data/access/lat/2yr\\_catalog](http://fermi.gsfc.nasa.gov/ssc/data/access/lat/2yr_catalog), the file we used is `gll_psc_v07.fit`

after subtracting the best estimate. We also mask out sources including Geminga, 3C 454.3, and LAT PSR J1836+5925 and large sources like Orion and the Magellanic Clouds as we did in the previous papers (Su et al. 2010; Su & Finkbeiner 2012), although they are unlikely to be a problem at  $E > 80$  GeV, where we are searching for lines.

We produce the exposure maps using the `gtltcube` and `gtexpcube2` tasks in the Fermi Science Tools. For bright sources, the exposure is set to zero for excised pixels. For the smoothed maps, both the count map and exposure map are smoothed, and then divided. At high energies, where the PSF is small, this effectively interpolates over the masked pixels.

### 3. A MODEL-INDEPENDENT SEARCH FOR LINE-EMITTING REGIONS

We begin by constructing maps in broad (20 GeV) energy bins and taking linear combinations that cancel most Galactic emission. This has the potential to reveal a component with an unusual spectrum in a model-independent way.

In Figures 1 and 2, we show the full sky map in four energy bins in the range 100 to 180 GeV, using CLEAN and SOURCE events, respectively. Even after nearly four years of observation, the number of gamma-ray photons

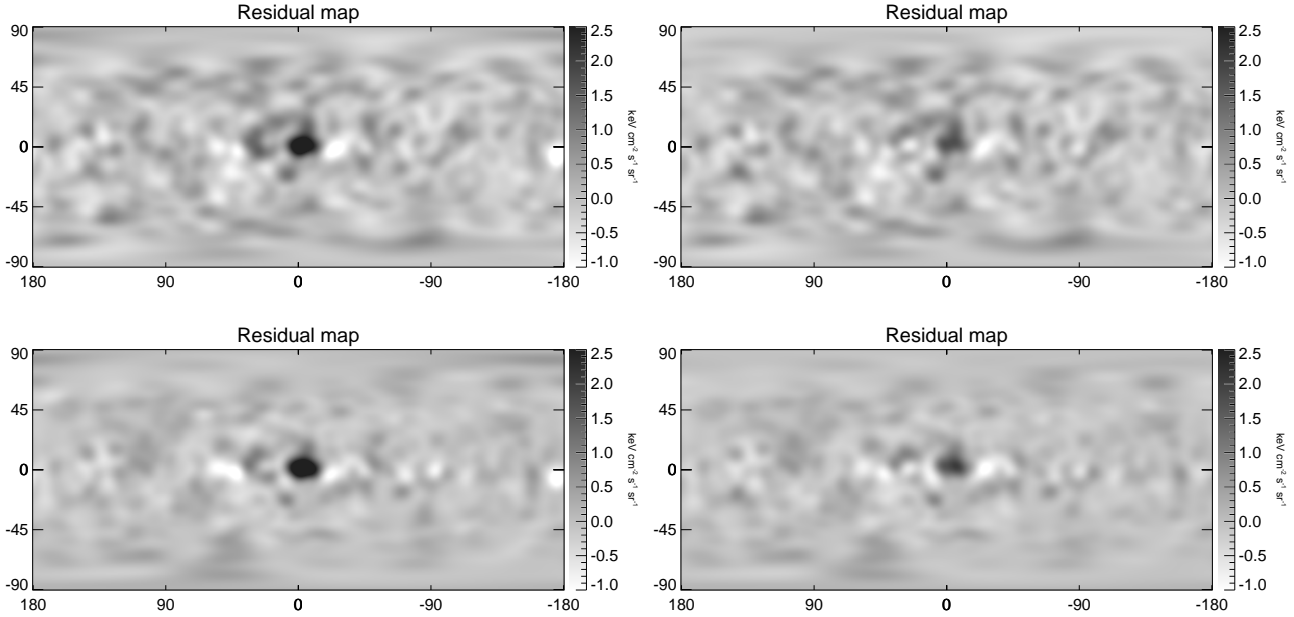


FIG. 5.— Residual maps the same as the *lower right* panel of Figures 3 and 4, but using SOURCE events before (*upper left* panel) and after (*upper right* panel) point source subtraction, or using ULTRACLEAN events before (*lower left* panel) and after (*lower right* panel) point source subtraction.

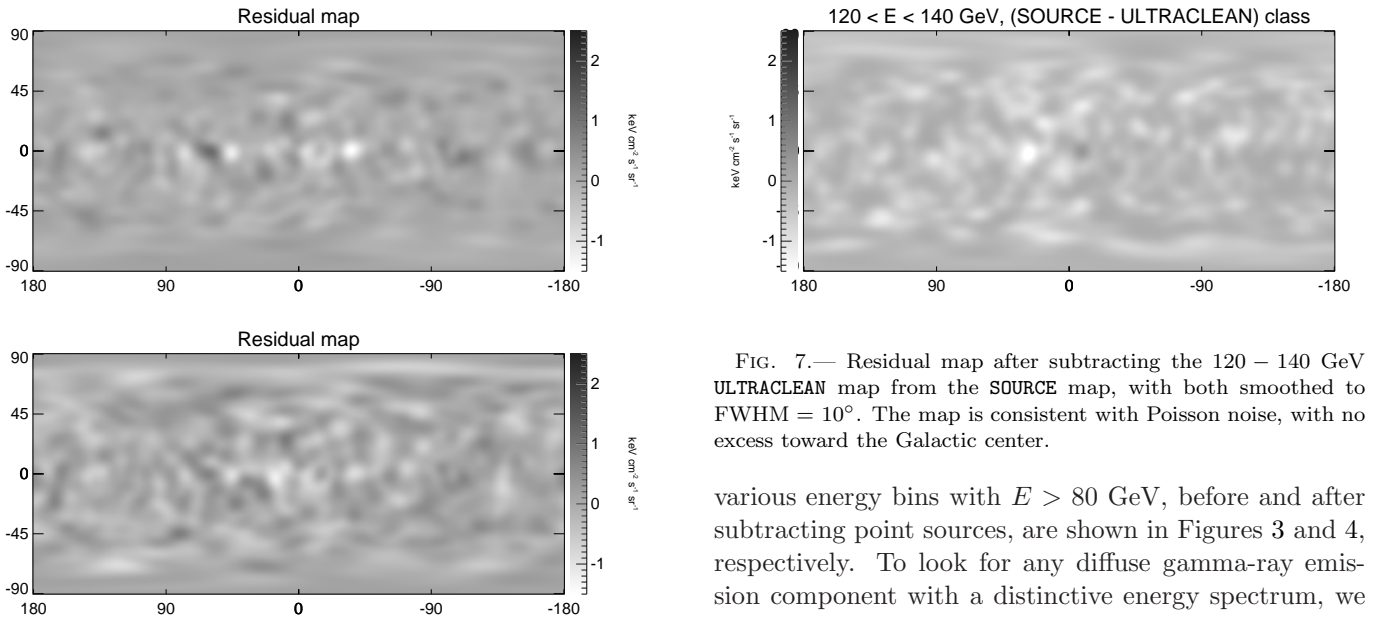


FIG. 6.— Residual maps by subtracting the average map of 100 – 120 GeV and 140 – 160 GeV maps from the average map of 80 – 100 GeV and 160 – 180 GeV maps (individual maps are shown in Figure 3). Most of the large scale diffuse gamma-ray structures (including the Galactic plane) and bright point sources have been removed, and *no* gamma-ray cuspy structure toward the Galactic center is visible in the residual gamma-ray maps. The maps are constructed using *Fermi*-LAT 3.7 year CLEAN events (*upper panel*) and SOURCE events (*lower panel*), respectively.

with  $E \gtrsim 100$  GeV is still quite limited and the maps are Poisson noise dominated. In order to inspect diffuse gamma-ray structure, we smooth the maps with a Gaussian kernel of  $\text{FWHM} = 10^\circ$ . Smoothed CLEAN maps in

FIG. 7.— Residual map after subtracting the 120 – 140 GeV ULTRACLEAN map from the SOURCE map, with both smoothed to  $\text{FWHM} = 10^\circ$ . The map is consistent with Poisson noise, with no excess toward the Galactic center.

various energy bins with  $E > 80$  GeV, before and after subtracting point sources, are shown in Figures 3 and 4, respectively. To look for any diffuse gamma-ray emission component with a distinctive energy spectrum, we examine various linear combinations of maps that cancel out the Galactic plane emission and visually inspect the residual maps.

Interestingly, when we subtract the average map (averaged in  $E^2 dN/dE$  units) of the 80 – 100 GeV, 100 – 120 GeV, 140 – 160 GeV, and 160 – 180 GeV maps from the 120 – 140 GeV map, most of the large scale diffuse gamma-ray structures (including the relatively bright Galactic plane) and visible point sources have been largely removed. However, a resolved cuspy structure toward the inner Galaxy with a size slightly larger than the smoothing kernel is revealed as the only visible structure in the residual gamma-ray map. We have repeated the analysis only subtracting 80 – 100 GeV and 100 – 120

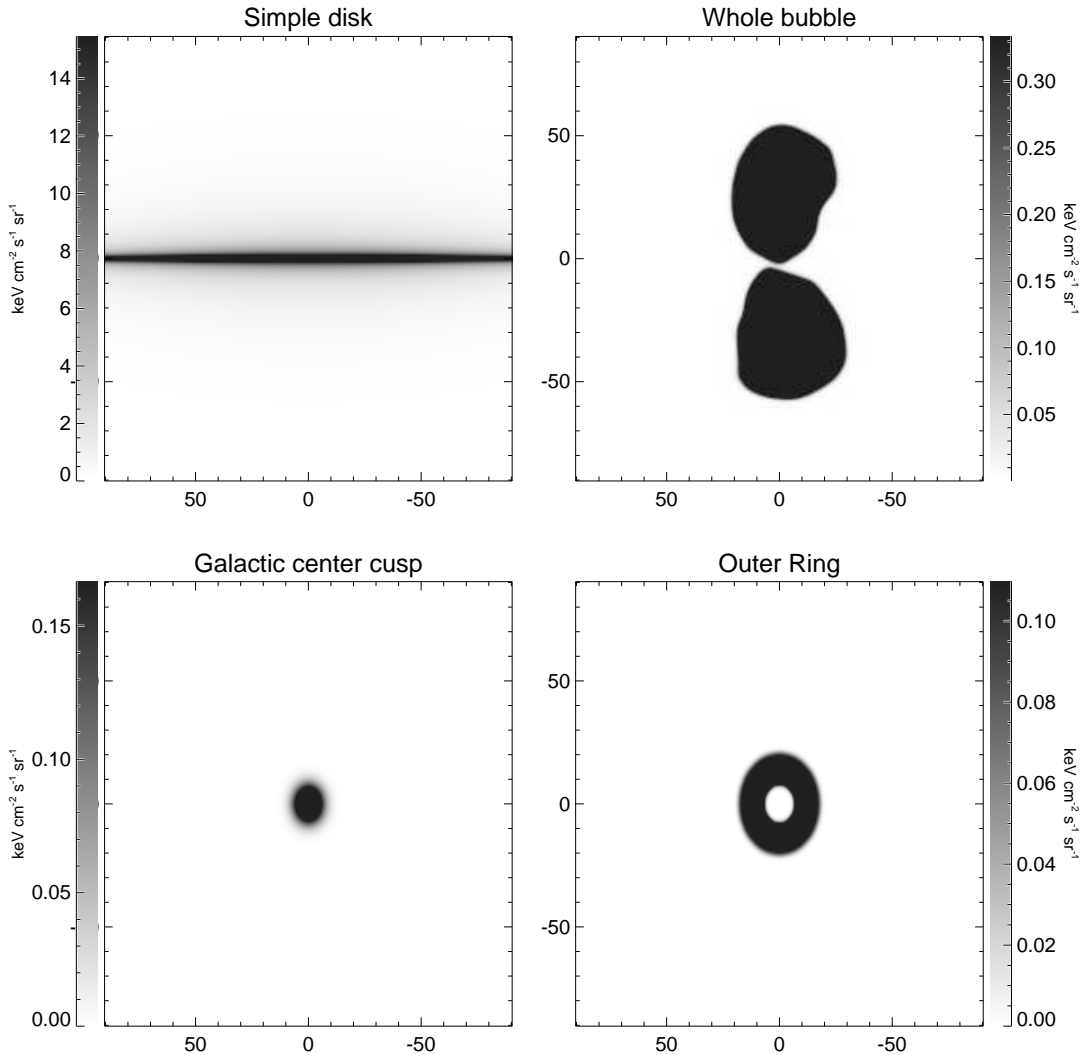


FIG. 8.— Spatial templates used in the Poisson likelihood analysis. *Upper left*: Galactic disk template, *upper right*: *Fermi* bubble template, *lower left*: gamma-ray cuspy template as a Gaussian distribution with FWHM =  $4^\circ$ , *lower right*: outer ring template as a Gaussian distribution with FWHM =  $10^\circ$ , but masking out the central region where the gamma-ray cuspy template is. In Figure 9 and Figure 11, we split the *Fermi* bubble template into two components one with  $|b| > 30^\circ$  and the other with  $|b| < 30^\circ$ .

GeV maps from the 120 – 140 GeV map, or only subtracting 140 – 160 GeV and 160 – 180 GeV maps, and we obtained similar residual structure toward the Galactic center. We also repeat this exercise using SOURCE and ULTRACLEAN event classes and the residual maps are shown in Figure 5. The GC excess is similar in each case, and the rest of the gamma-ray sky is consistent with Poisson noise. This excess at  $\sim 120 - 140$  GeV strongly suggests a novel diffuse gamma-ray component toward the Galactic center with unusual spectrum. Furthermore, this energy range coincides with the recently suggested tentative signature of gamma-ray excess at 130 GeV (Bringmann et al. 2012; Weniger 2012), which is under active debate in the literature (Boyarsky et al. 2012; Tempel et al. 2012; Profumo & Linden 2012). Assuming the distance to the Galactic center is  $R_\odot = 8.5$  kpc, the size of the gamma-ray cusp is  $\lesssim 1$  kpc.

We show in Figure 6 the difference map between the

average map of 80 – 100 GeV and 160 – 180 GeV maps and the average map of 100 – 120 GeV and 140 – 160 GeV maps. The difference map is consistent with Poisson noise and *no* diffuse gamma-ray excess toward the inner Galaxy is visible. In order to test whether the excess is due to residual cosmic ray contamination, we subtract ULTRACLEAN sky maps from SOURCE sky maps. This residual map should be mostly dominated by cosmic rays since a large fraction of the real gamma-ray photons have been removed. Indeed, Figure 7 demonstrates that there is no excess toward the inner Galaxy in this map, thus we can rule out the possibility that the central excess is due to cosmic ray contamination in the LAT data.

Toward the inner Galaxy, the *Fermi* bubbles extend  $\sim 50^\circ$  above and below the Galactic center, with a width of  $\sim 40^\circ$  in longitude. The gamma-ray emission associated with these bubbles has a significantly harder spectrum ( $dN/dE \sim E^{-2}$ ) than the inverse Compton emis-

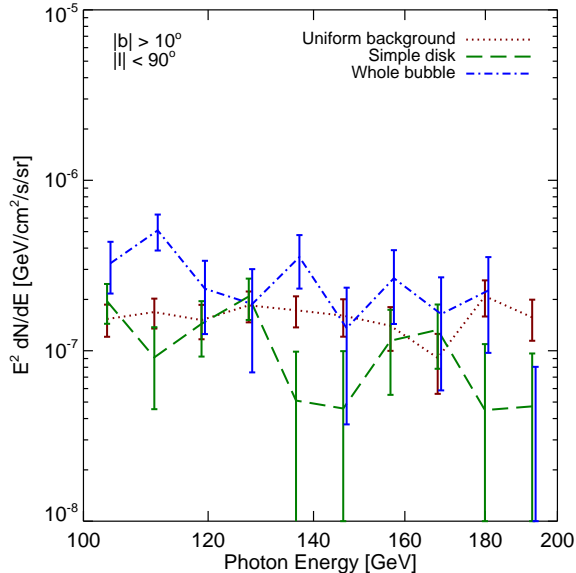


FIG. 9.— Spectral energy distribution of three diffuse gamma-ray templates. The disk-correlated emission (*green dashed*) approximately traces the inverse Compton and bremsstrahlung components. The spectrum of the uniform emission (*dotted brown line*) includes the isotropic part of the extragalactic background and cosmic-ray contamination. We have not included the dust-correlated emission or *Loop I* template as in Su et al. (2010), because the expected spectrum is softer and we do not expect a significant contribution from these components at  $E \gtrsim 100$  GeV. Vertical bars show the marginalized 68% confidence range derived from the parameter covariance matrix for the template coefficients in each energy bin.

sion from electrons in the Galactic disk, or the gamma-rays produced by decay of  $\pi^0$  from proton-ISM collisions. We note that the morphology of the resolved gamma-ray cusp has a different shape from the bubbles, and the bubble structure has been largely cancelled out and not visible in the residual maps (as shown in e.g. Figure 5). Thus we conclude that the new gamma-ray cusp has no obvious connection with the bubbles. We will also demonstrate this more explicitly in Section 4.

#### 4. ENERGY SPECTRUM OF THE GAMMA-RAY CUSP

In §3 we argued for the existence of an excess with a concentrated cuspy shape in the GC at  $E = 120 - 140$  GeV. This motivates a more careful investigation of the energy spectrum and spatial distribution of the emission.

##### 4.1. Template regression

As in our previous work (e.g., Su et al. 2010), we consider linear combinations of spatial templates and compute the likelihood that the gamma-ray maps are described by a given linear combination. We fit a coefficient for each emission component using a multi-linear regression of simple templates, one energy bin at a time. This technique provides an estimate of the energy spectrum of each component using as few physical assumptions as possible.

By combining results from 16 logarithmically-spaced energy bands from 85 GeV to 200 GeV, we determine the spectral energy distribution for each component. In each fit, we model the “conventional” emission using three simple templates: a Galactic disk model, the *Fermi* bubbles, and a uniform background. The Galactic disk template has the functional form  $(\csc |b|) - 1$  in latitude and is a Gaussian ( $\sigma_\ell = 80^\circ$ ) in longitude, as in Su et al. (2010). The disk model mostly accounts for gamma rays from the Galactic plane including those produced by point sources, ISM emission ( $\pi^0$  and Bremsstrahlung) and inverse Compton scattering. The uniform background template absorbs the isotropic background due to extra-galactic emission and misclassified charged particle contamination, including heavy nuclei at high energies. We show maps of these templates in Figure 8.

For each set of model parameters, we compute the Poisson log likelihood,

$$\ln \mathcal{L} = \sum_i k_i \ln \mu_i - \mu_i - \ln(k_i!), \quad (1)$$

where  $\mu_i$  is the model counts map (i.e., linear combination of templates times exposure map) at pixel  $i$ , and  $k$  is the map of observed counts. The last term is a function only of the observed maps. We compute parameter errors in the Gaussian approximation by inverting the matrix of second partial derivatives of  $-\ln \mathcal{L}$  to obtain the covariance matrix, and taking the square root of the diagonals. The  $1\sigma$  Gaussian error corresponds to  $\Delta \ln \mathcal{L} = 1/2$ .

Template-correlated spectra for the 3-template fit are shown in Figure 9. The energy spectra show no significant deviation from a power law for any of the three components. This fact, together with the distinct spatial morphology of the gamma-ray cusp suggests the need to include a cusp template (shown in Figure 8) in the model. Inclusion of this template barely alters the derived spectrum of the first three components, but yields significant coefficients for the cusp from 110 to 140 GeV (Figure 10 and Table 1). The fact that the bubble coefficients show no such bump indicates that the bubble structure is unrelated to the  $\sim 130$  GeV excess. We find that the surface brightness of the center of the cusp is nearly two orders of magnitude greater than that of the *Fermi* bubble structure, but only over a limited energy range.

In Figure 10, we have done the fit with two different spatial masks: one excludes  $|b| < 1^\circ$  to avoid contamination from the Galactic disk close to the plane and the Galactic center (including the Galactic “ridge”); another one excludes much more of the Galactic disk with  $|b| < 5^\circ$  and  $|l| > 6^\circ$  without masking the Galactic center region. We have obtained similar results for both data cuts. The cusp structure emits gamma rays with a luminosity of  $(3.2 \pm 0.6) \times 10^{35}$  erg/s or  $(1.7 \pm 0.4) \times 10^{36}$  photons/sec. The null hypothesis of zero intensity of the cusp component is ruled out by  $5.0\sigma$ . Given the energy resolution

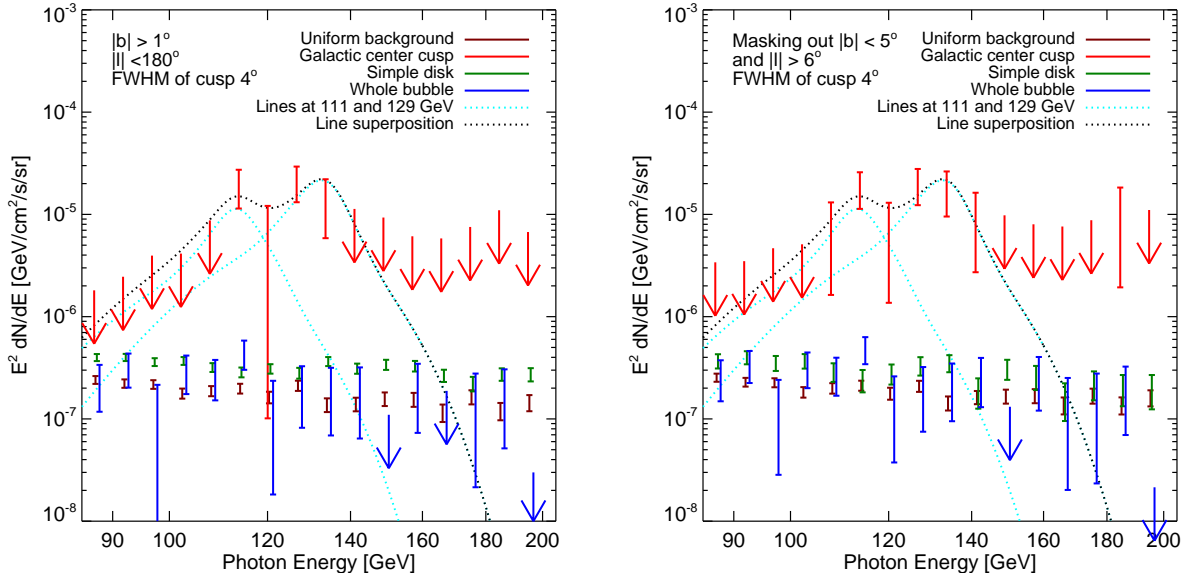


FIG. 10.— *Left panel*: Spectral energy distributions of the templates listed in the figure legend. In the *left panel*, we use CLEAN events with  $|b| > 1^\circ$  and all longitudes. Besides the disk-correlated emission (*green*), uniform emission (*brown*), and the *Fermi* bubble template (*blue*), the cusp component modeled as a FWHM =  $4^\circ$  Gaussian in the GC (*red*) has been included. Vertical bars show the marginalized 68% confidence range derived from the parameter covariance matrix for the template coefficients in each energy bin. Arrows indicate  $1\sigma$  upper limits. For reference, we overplot lines centered at 111 GeV and 129 GeV (*dotted cyan*) convolved with a three-Gaussian approximation of the LAT instrumental response (Edmonds 2011), and their sum (*dotted black*). The line centers and amplitudes are determined from a fit to the spectrum in the right panel (see text). *Right panel*: the same as the left panel but using data masking out  $|b| < 5^\circ$  and  $|l| > 6^\circ$ .

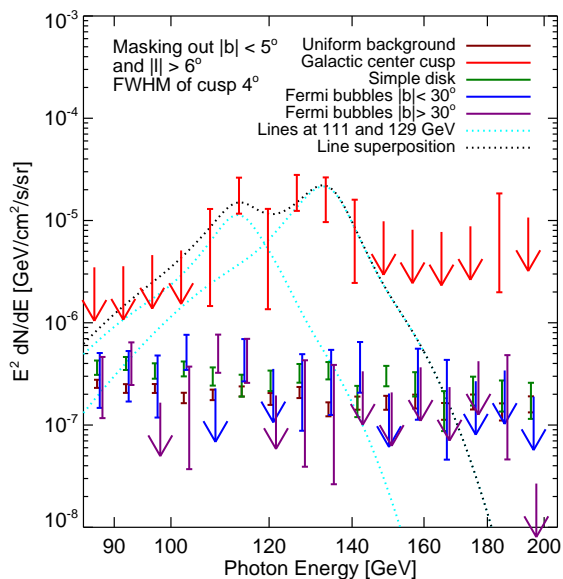


FIG. 11.— Same as right panel of Figure 10 but splitting the bubble template into two regions one with  $|b| > 30^\circ$  and the other with  $|b| < 30^\circ$ .

of the *Fermi*-LAT at  $E \gtrsim 100$  GeV, the spectral excess at  $110 \lesssim E \lesssim 140$  GeV is consistent with emission from one or two lines after considering the line-spread function (LSF) (Edmonds 2011), which strongly suggests the novel nature of the gamma-ray cusp as no known astrophysical process can produce this feature. Except for unexpected instrumental systematics or an increasingly

unlikely statistical fluke, a dark matter annihilation signal from the inner Galaxy is the most likely explanation. In another variant of the fit, we split the bubble template into two independent components in the fitting, high latitude ( $|b| > 30^\circ$ ) and low latitude ( $|b| < 30^\circ$ ). The purpose is to demonstrate that the low latitude bubble is also independent from the gamma-ray cusp. Again, we find no sign of a bump in the spectra of other diffuse gamma-ray components, but the cusp has a spectrum with an excess at 110 – 140 GeV and is consistent with zero in the other bins (Figure 11). Instead of using CLEAN class, we have tried using SOURCE class for the likelihood analysis, and obtained similar results (Figure 12).

The energy spectrum of the cusp is consistent with a single spectral line (at energy  $127.0 \pm 2.0$  GeV with  $\chi^2 = 4.48$  for 4 d.o.f.). But a pair of lines at  $110.8 \pm 4.4$  GeV and  $128.8 \pm 2.7$  GeV provides a marginally better fit (with  $\chi^2 = 1.25$  for 2 d.o.f.). We have compared the best fit one line and two line profile with the measured energy spectrum in Figure 13. The observation is compatible with a  $140.8 \pm 2.8$  GeV WIMP annihilating through  $\gamma Z$  and  $\gamma h$  assuming  $m_h = 125$  GeV (with  $\chi^2 = 3.33$  for 3 d.o.f.) or a  $127.3 \pm 2.7$  GeV WIMP annihilating through  $\gamma\gamma$  and  $\gamma Z$  (with  $\chi^2 = 1.67$  for 3 d.o.f.) (e.g., Weiner & Yavin 2012).

The gamma-ray cusp appears to possess a symmetric distribution around the Galactic center. To investigate whether there is any more extended cusp component contributing the excess at 120 – 140 GeV, we include an extra “outer ring” template as shown in Figure 8. The



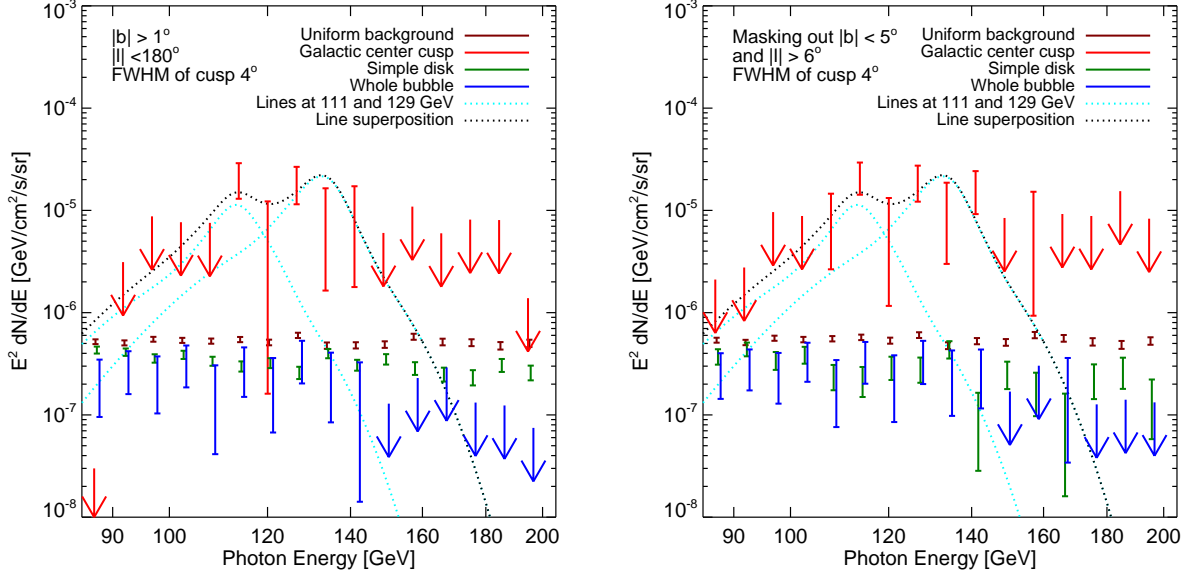


FIG. 12.— Same as Figure 10 but using SOURCE events instead of CLEAN. The level of the uniform background is more than a factor of 2 higher than that shown in Figure 10. However, the resulting energy spectrum of the gamma-ray cusp (red dashed line) is quite similar to that shown in figures 10 and 11.

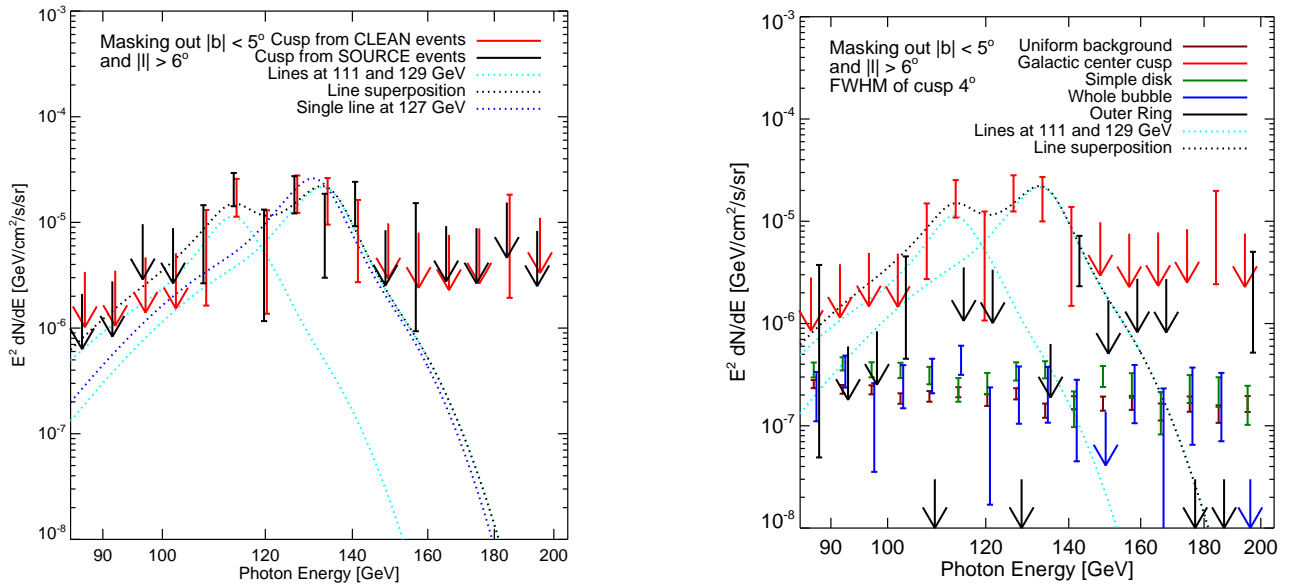


FIG. 13.— Same as right panel of Figure 10 but overplot the best fit one gamma-ray line profile convolved with the instrument response, and compared with the best fit two-line profile.

outer ring template is a FWHM=10° Gaussian with an 8° radius hole in the center. Even with this freedom, there is no significant change in the cusp spectrum (Figure 14). There was no significant improvement of the likelihood for this model, and the spectrum of the outer ring is consistent with zero. Our conclusion is that the gamma-ray cusp is a distinct component, and is centrally concentrated.

#### 4.2. Trials factor

FIG. 14.— Same as right panel of Figure 10 but including extra outer ring template.

We use a trials factor of 300 for the single-line fits centered on the Galactic center, and 6000 for fits that are off center. This choice is based on the fact that the LAT energy resolution is  $\sim 10\%$  over most of the energy range, and a line anywhere from 1 to 300 GeV would have been just as impressive, yielding 60 energy bins. Furthermore, a broader line (or two lines near each other) has an additional trials factor. We allow an extra factor of 5, giving us 300.

For fits that recenter the cusp in  $\ell$ , we would have considered any center with  $|\ell| < 5^\circ$  interesting, and the

E range (GeV)	Energy	cusps (CLEAN)	cusps (SOURCE)
84.9 – 89.5	87.2	-1.01 ± 4.42	-2.19 ± 4.30
89.5 – 94.5	92.0	-0.79 ± 4.28	-1.53 ± 4.29
94.5 – 99.7	97.1	0.03 ± 4.64	4.37 ± 5.26
99.7 – 105.2	102.4	0.06 ± 5.04	3.05 ± 5.77
105.2 – 111.0	108.1	7.37 ± 5.73	8.61 ± 5.95
111.0 – 117.1	114.0	18.58 ± 7.25	21.80 ± 7.57
117.1 – 123.6	120.3	7.18 ± 5.82	7.19 ± 6.03
123.6 – 130.4	127.0	20.06 ± 7.75	19.78 ± 7.61
130.4 – 137.6	134.0	17.91 ± 8.38	10.82 ± 7.83
137.6 – 145.2	141.4	9.50 ± 6.78	16.71 ± 7.50
145.2 – 153.2	149.2	4.07 ± 5.73	3.07 ± 5.36
153.2 – 161.7	157.4	1.70 ± 6.29	8.07 ± 7.14
161.7 – 170.6	166.1	3.11 ± 4.50	4.34 ± 4.88
170.6 – 180.1	175.2	3.08 ± 5.69	2.91 ± 5.90
180.1 – 190.0	185.0	10.11 ± 8.18	7.07 ± 8.34
190.0 – 200.5	195.2	3.99 ± 7.04	1.84 ± 6.46

TABLE 1

THE TEMPLATE FITTING COEFFICIENTS AND ERRORS OF THE DIFFUSE GAMMA-RAY CUSP CORRESPOND TO THE RIGHT PANEL OF FIGURE 10 AND RIGHT PANEL OF FIGURE 12. THE GAMMA-RAY LUMINOSITY IN EACH ENERGY RANGE IS SHOWN IN THE UNIT OF  $\text{keV cm}^{-2}\text{s}^{-1}\text{sr}^{-1}$ .

centering must change by  $\pm 0.25^\circ$  to make unit change in  $TS$ , so we take there to be 20 interesting spatial bins. For single-line, off-center fits we use a trials factor of 6000.

The local significance of the centered Gaussian template is  $5.0\sigma$ , obtained by summing the significance of each bin in quadrature (Table 1). After diluting the  $p$  value corresponding to  $5.0\sigma$  by a factor of 300, we obtain a significance corresponding to  $3.7\sigma$ . We note that, if the line is real, an additional 40% more data will be enough to obtain a  $5.0\sigma$  detection, even with the trials factor of 300.

The previous trials factor is for a line *anywhere* with a range of widths. On the other hand, if one asserts that the line pair is from  $\gamma\gamma$  and  $\gamma Z$  dark matter annihilation channels, the trials factor can be calculated as follows:

The two  $\gamma$  lines could have been anywhere between the  $Z$  mass and 300 GeV. There are 12 log-spaced bins of width 10% in that range. Also, there is no additional trials factor for a width; we simply have two lines, and we let their two amplitudes float as a free parameter, as well as the WIMP mass. There is also a factor from the number of line-producing scenarios: we could have seen a single line or two lines from  $\gamma\gamma$  and  $\gamma Z$  or  $\gamma Z$  and  $\gamma h$ . Considering these 3 scenarios, we assign a trials factor of 36 for the single-line fits. For off-center fits, we use  $36 \times 20 = 720$ .

## 5. DETAILED SPATIAL PROFILE OF THE CUSP

The cusp template used in Section 4 is assumed to be centered on the GC, and the choice of  $4^\circ$  FWHM is somewhat arbitrary. We would like the data tell us what template to use, but there are so few photons, it is difficult to make sense of an unsmoothed map of counts. However, the smoothed maps indicate the cusp is slightly off center (to the W of the GC) and it is essential to follow

this up.

In this section, we consider individual photon events (not maps) and assume the exposure across the GC is slowly varying. We project the event locations into histograms of  $\ell$  and  $b$  and study the distributions, finding parameters of a best-fit Gaussian. In this way, we may find the location, shape, and significance of the 130 GeV feature in a way that is independent of the previous sections, though somewhat less principled because we do not explicitly use the exposure map. We will not use the results of this section to raise our claimed significance, but rather to emphasize that the cusp is centrally concentrated, has a sharp spectrum, and is somewhat off center.

We model the background spectrum to be  $dN/dE \propto E^{-2.6}$ , with the amplitude in each bin set by the 10-50 GeV average. The exposure map is a weak function of position and energy, and we neglect that variation in this analysis. An index of  $-2.5$  gives a significantly worse fit by overestimating counts at 100 to 200 GeV. The  $\pi^0$  emission is closer to  $-2.7$  at lower energies, but  $-2.6$  is a conservative choice, because assuming lower background at 130 GeV would make any excess more significant.

We consider two spatial projections of the photon distribution in the inner Galaxy. For the longitude projection, we project the region  $|\ell| < 10^\circ$ ,  $|b| < 5^\circ$ , in  $0.5^\circ$  bins of  $\ell$  yielding a nearly flat distribution (blue line in top panels of Figure 15). For the latitude distribution, we project the region  $-5 < \ell < 2$ ,  $|b| < 10$ , in  $0.5^\circ$  bins of  $b$ , finding the emission near the plane dominates (bottom panels of Figure 15). From this we immediately see that the Galactic plane is much brighter than elsewhere, but the Galactic center is *not* particularly brighter than elsewhere in the plane at 10 to 50 GeV.

In order to test for the existence of a bump, we compare the  $\ln \mathcal{L}_0$  for the null hypothesis to a model with an additional Gaussian of FWHM  $F_\ell$ , centered at  $\ell_0$  with peak height  $A_\ell$ . We compute  $\Delta \ln \mathcal{L} \equiv \ln(\mathcal{L}/\mathcal{L}_0)$  and express results using the test statistic (Mattox et al. 1996),  $TS = 2\Delta \ln \mathcal{L}$ . The test statistic plays the role  $\Delta\chi^2$  would play in a Gaussian problem.

In comparing the  $\ln \mathcal{L}$  of two models, one must account for the fact that the two models reside in different parameter spaces. In our case, the null model space is a subspace of the other with 3 fewer parameters, obtained by setting  $A_\ell$  to zero. In this case, the  $TS$  distribution is simply the  $\chi^2$  distribution for 3 degrees of freedom.

Using photons from all incidence angles, the addition of a Gaussian improves the  $TS$  by 36. This is *not* a  $6\sigma$  result because of the 3 additional degrees of freedom. Rather, the probability that  $TS$  would be 36 or higher is  $p = 7.5 \times 10^{-8}$ , corresponding to  $5.25\sigma$  local significance (not including the global trials factor). The parameters of the Gaussian are  $F_\ell = 1.4_{-0.4}^{+1.6}$ ,  $\ell_0 = -1.5 \pm 0.3$ , and an amplitude corresponding to 14.0 photons (red line,

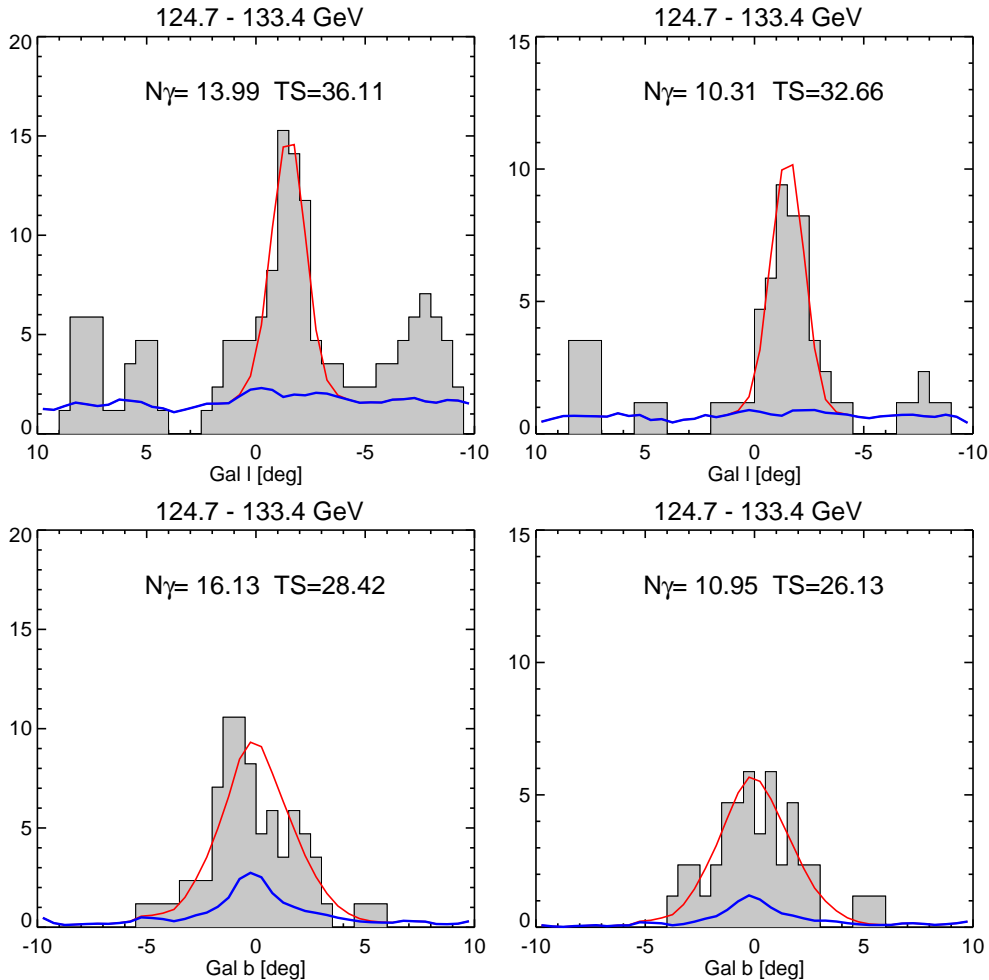


FIG. 15.— Profiles for both  $\ell$  and  $b$ . Even though the high-incidence-angle photons ( $\theta > 40^\circ$ ; right) panels have half the exposure (9.7% vs. 19% for the left panels), they have more than half of the photons, and nearly the same  $TS$  due to lower off-line background leaking in. This demonstrates the statistical power of the high-incidence photons for line detection. See section 5 for a discussion of the significance.

Figure 15).

In the latitude direction, the fit is complicated by the concentration of conventional continuum emission in the plane. The cusp is not significantly offset in the  $b$  direction, but sits in the region of highest background, so addition of the cusp is not demanded as strongly by the fit. We introduce two new degrees of freedom, the amplitude and FWHM of a Gaussian centered at  $b_0 = 0$ . This yields  $TS = 28.4$  and  $p = 6.8 \times 10^{-7}$ , corresponding to  $4.8\sigma$  (local significance). The maximum likelihood parameters of the Gaussian are  $F_b = 3.9^{+1.5}_{-0.7}$  and  $A_b$  corresponding to 16.1 photons. Both the  $\ell$  and  $b$  fits are roughly compatible with  $\text{FWHM} = 3^\circ$ , but there is a slight preference for an elongation of the cusp in the  $b$  direction. A careful study of this will require much more data.

In Figure 15 (right panels) we also display the same plots for the high-incidence sample ( $\theta > 40^\circ$ ). See Figure 16 for such plots in 30 energy bins. The high-incidence-angle subsample contains half of the exposure time (9.7% vs. 19%) but due to better energy resolution ( $\Delta E/E \sim 0.06$ ) has less background on the line, and therefore yields a  $TS$  almost as large as the full data. In this sense, *most*

*of the  $TS$  results from high  $\theta$  events.* This subsample would have yielded  $TS = 32.6$  ( $p = 3.9 \times 10^{-7}$ ,  $4.93\sigma$ ) for the  $\ell$  profile, and  $TS = 26.1$  ( $p = 2.2 \times 10^{-6}$ ,  $4.59\sigma$ ) for the  $b$  profile. Although these are slightly worse  $p$  values than for the full data, they may actually be more persuasive due to the lower background.

The fact that the cusp appears to be significantly off center implies that our spectral fit in the previous section erred by using a centered cusp template. In Figure 17 we show the measured energy spectrum of a  $3^\circ$  FWHM cusp template, centered at  $\ell = -1.5^\circ$  and  $b = 0^\circ$ . The local significance of this fit is  $5.5\sigma$  relative to the null hypothesis of zero intensity. This improvement is heartening; however, because of the extra parameter, the trials factor is now larger, diluting the significance.

## 6. VALIDATION TESTS

### 6.1. Assessment of line profile

In section 4, we investigated the cusp emission by analyzing maps in various energy bins. This allowed a separation of spectral components by morphology, but relied on an arbitrary choice of binning. The result – that there

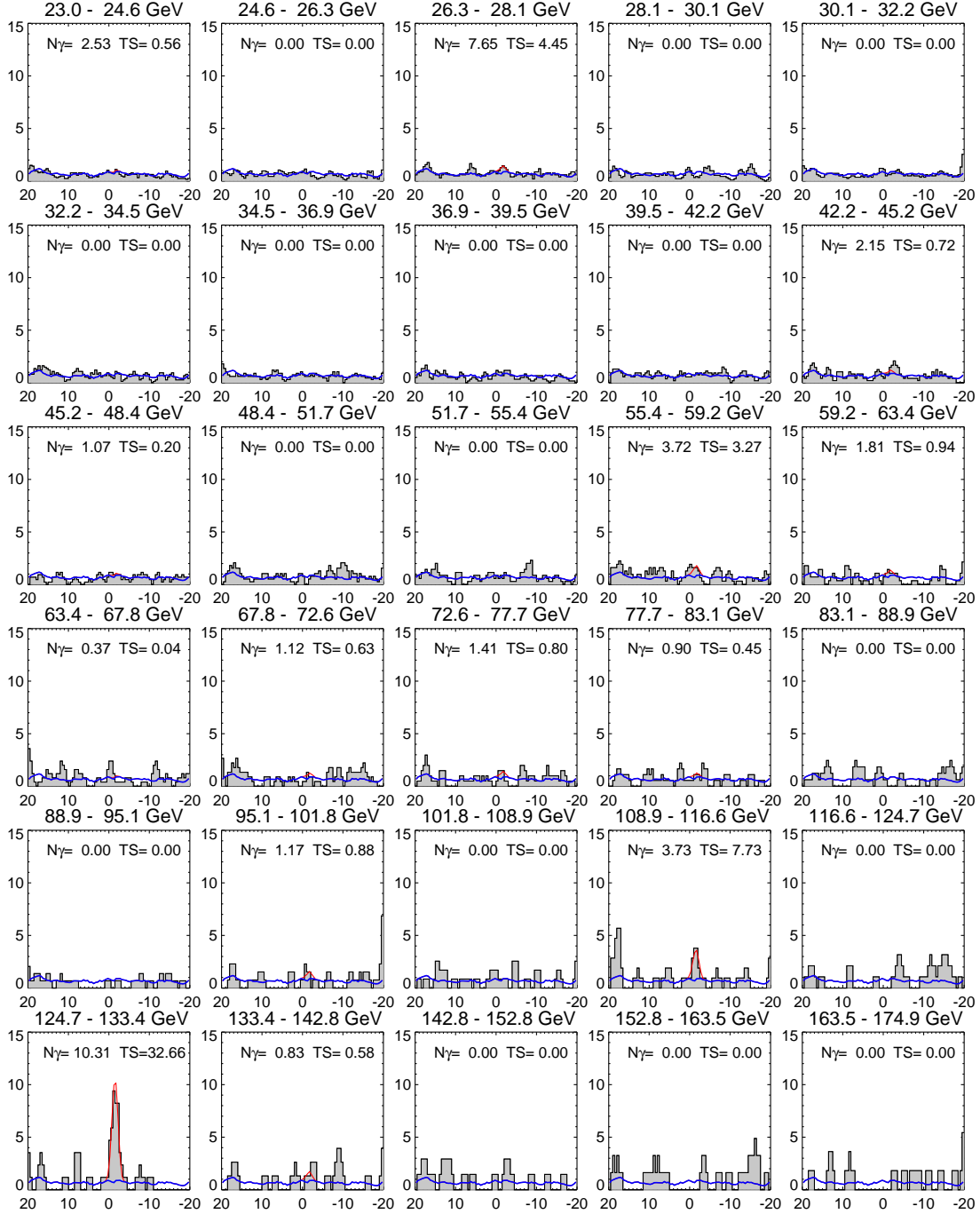


FIG. 16.— Profile of high-incidence photon ( $\theta > 40$  deg) longitude distribution for  $|b| < 5^\circ$ . The  $0.5^\circ$  bins have been smoothed by a 3-bin box, and rescaled to arbitrary units of  $E^{2.6}dN/dE$ , making the background disk emission constant with  $E$ . The background (blue) is the average in these units for  $10 < E < 50$  GeV. In each panel, the (non-negative) amplitude of a  $\text{FWHM}_\ell = 1.4^\circ$  Gaussian centered at  $\ell = -1.5$  is fit by maximizing the Poisson likelihood. The corresponding number of photons and test statistic (TS) are displayed. The only energy bin with significant emission is the 124.7-133.4 bin, centered on 129 GeV. See text for discussion of significance. The bin centered on 113 GeV is not significant by itself, but is compatible with a line strength of 1/3 to 1/2 that of the putative 129 GeV line.

is a cusp of emission in the inner Galaxy – motivates an unbinned analysis of this region.

In an unbinned analysis, one dispenses with arbitrary binning choices (size and shift) and instead analyzes individual photon events. For example, the parameters of a well defined model may be estimated with no binning in space or energy. In the absence of a principled model, a compromise technique is to convolve a finely binned en-

ergy histogram with some kernel and compare profiles of prospective lines with those expected for a true line, i.e. the instrumental response convolved with the smoothing kernel.

In the case of LAT data this allows us to do an interesting reality check. Energy resolution of events at high incidence angle ( $\theta \sim 60^\circ$ ) is a factor of  $\sim 2$  better than that of normal-incidence photons, motivating the

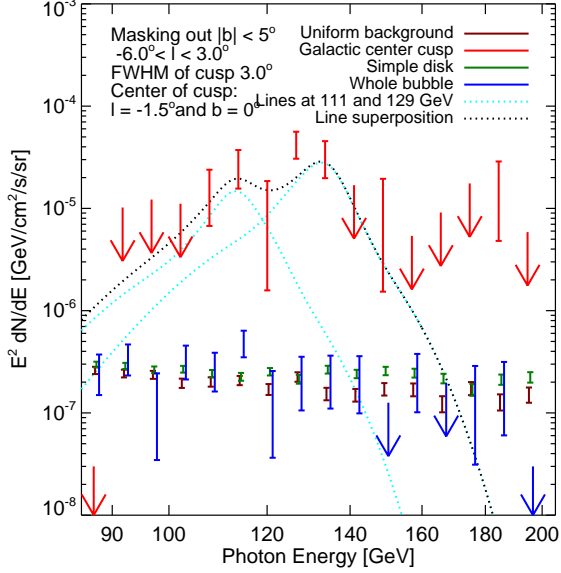


FIG. 17.— Same as right panel of Figure 10 but with the cusp template centered at  $\ell = -1.5^\circ$  and  $b = 0^\circ$ .

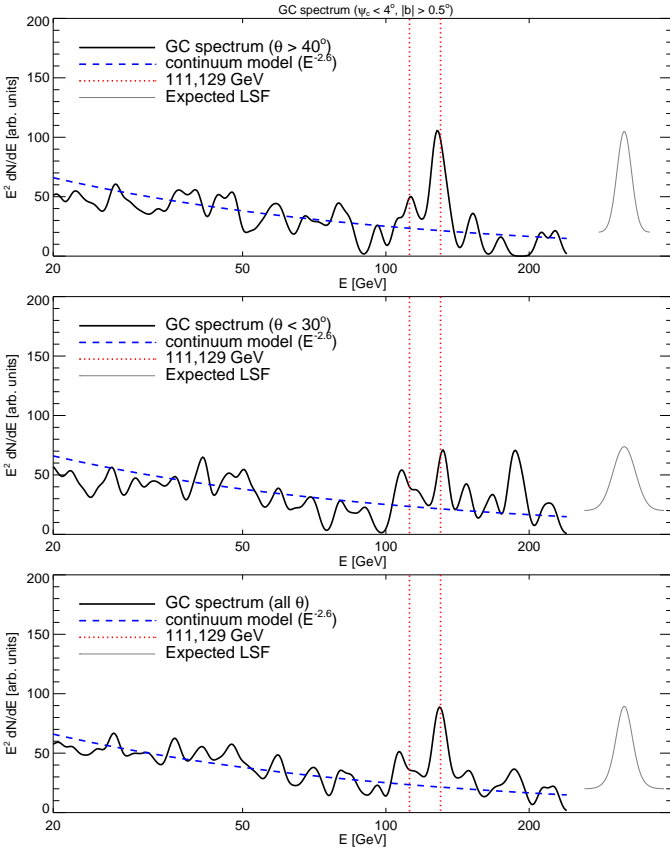


FIG. 18.— Spectrum of emission within  $4^\circ$  of the cusp center  $(\ell, b) = (-1.5, 0)$ , excluding  $|b| < 0.5^\circ$ . High-incidence angle events (*upper panel*) have a factor of  $\sim 2$  better energy resolution than those that enter the LAT close to normal incidence (*middle panel*) or the whole sample (*lower panel*). All three spectra have been smoothed by a Gaussian of 0.06 FWHM in  $\Delta E/E$ , similar to the expected resolution of the upper panel. The continuum model is  $dN/dE \sim E^{-2.6}$ , normalized at  $20 < E < 50$  GeV (*blue dashed*).

following test.

We select low incidence ( $\theta < 30^\circ$ ) and high incidence ( $\theta > 40^\circ$ ) photon samples. We restrict to those near the cusp center at  $(\ell, b) = (-1.5, 0)$  ( $\psi_c < 4^\circ$ ) but not in the plane ( $|b| < 0.5^\circ$ ). We then convolve each with a kernel and compare them (Figure 18). We adopt an LSF with a FWHM of  $\Delta E/E = 0.06$  for high incidence and 0.12 for low incidence (Edmonds 2011), and in both cases convolve with another FWHM 0.06 Gaussian. After convolution, the LSF is FWHM 0.085 for high incidence and 0.134 for low incidence. Normalized Gaussians of these widths are shown for reference, normalized to the expected line strength at 130 GeV. Maps constructed using only high incidence events are shown in Figure 19.

Note that:

- The 129 GeV feature shape is strikingly similar to that expected for a line. The 111 GeV feature is unconvincing, but is also compatible with a line.
- In some cases, fluctuations appear, but are not present in both low and high incidence spectra.

This analysis did introduce some additional parameters, but we have made natural choices for them: The 68% containment radius of the cusp is approximately  $4^\circ$ , the Galactic ridge is about  $0.5^\circ$  thick, and the  $\Delta E/E = 0.06$  smoothing kernel is similar to the LSF of the LAT at high incidence. Smoothing a spectrum by its LSF is often a good compromise between resolution and noise suppression in the high-noise limit. Because these parameters are all fixed to natural values, there is no significant trials factor for this test, apart from the obvious one, that the lines could have appeared anywhere (Section 4.2).

This test did not have to succeed. The fact that the high-incidence photon sample has sharper spectral features is important; if the high- $\theta$  and low- $\theta$  spectra in Figure 18 had been reversed, it would have been devastating for the line hypothesis.

### 6.2. Null test: Galactic plane spectrum

To emphasize that the line feature in Figure 18 appears near the Galactic center and not elsewhere, we perform the same analysis on the Galactic plane ( $|b| < 2^\circ$ ) away from the GC ( $\psi > 5^\circ$ ). We find no indication of a line in either high-incidence or low-incidence photons (Figure 20).

### 6.3. Null test: Earth emission photons

Another null test is provided by the Earth emission photons. Cosmic-ray induced cascades in the Earth's atmosphere shower photons on the LAT at high zenith angle ( $Z > 108^\circ$ ). These provide another null test, as there is no reason for there to be a 130 GeV feature in the Earth emission spectrum. On average, no feature is seen (Figure 21). However, there is a hint of a line at 130 GeV in the low-incidence events and one at 111

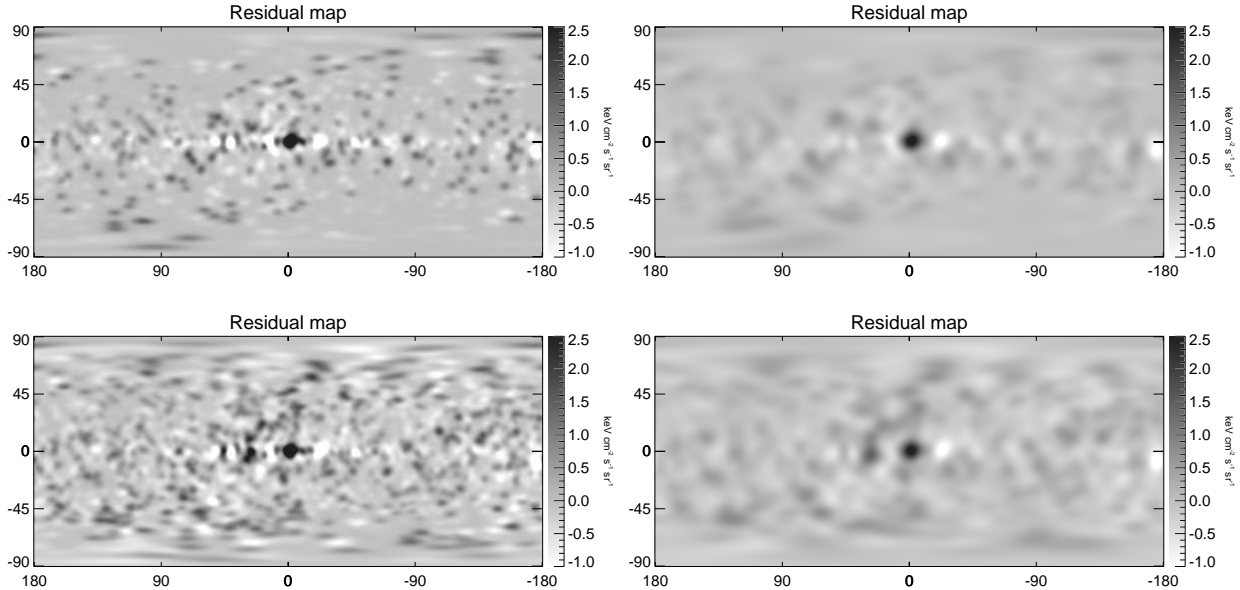


FIG. 19.— Same as Figure 5, but using only events with high incidence angle  $\theta > 40^\circ$  which has better energy resolution. The maps have been smoothed to  $5^\circ$  (left two panels) and  $10^\circ$  (right two panels), and use CLEAN event class (upper two panels) and SOURCE event class (lower two panels). The resolved gamma-ray cusp structure is centered  $1.5^\circ$  W of the Galactic center.

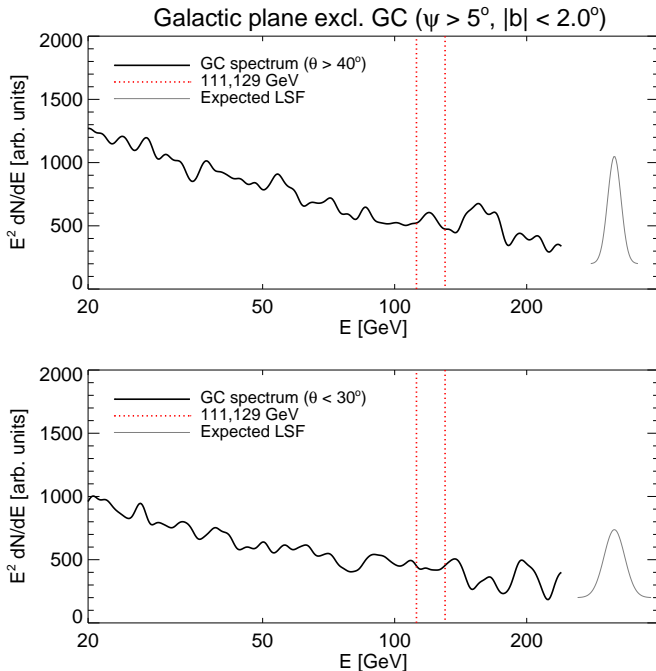


FIG. 20.— Like Figure 18, except for  $|b| < 2^\circ$  excluding photons within  $5^\circ$  of the Galactic center. There is no indication of a spectral feature near 130 GeV in the Galactic plane away from the Galactic center.

GeV in the high-incidence events. These features also require a trials factor, but if they turn out to be robust, then serious concerns would be raised about instrumental artifacts giving rise to the observed lines.

## 7. FITTING WITH DARK MATTER PROFILE

In previous sections, we have modeled the line emission cusp with a Gaussian in an attempt to keep the analysis generic. However, WIMP annihilation is the most likely

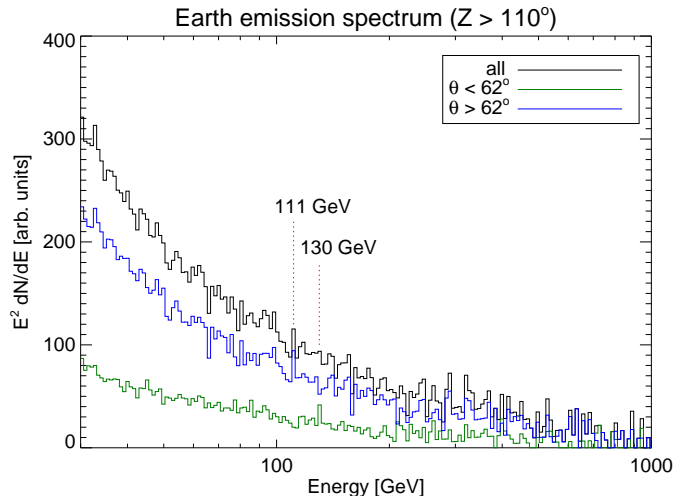


FIG. 21.— Photons from cascades in the Earth’s atmosphere (sometimes incorrectly called “albedo” photons), and with  $10^\circ$  of the GC, show a slight excess at 111 and 130 GeV also. Because these photons arrive at high zenith angle ( $Z > 110^\circ$ ), they tend to have a high incidence angle (median  $\theta = 63.2^\circ$ ). The low- $\theta$  photons show a small bump at 130 GeV, and the high- $\theta$  photons show a small bump at 111 GeV. The cuts were chosen to maximize these features, so interpretation of this plot requires a modest trials factor.

explanation for gamma-ray line emission, and we would like to know if the signal expected from a reasonable DM profile fits the data better than a Gaussian. In this section, we repeat our template analysis with an Einasto profile as well as a set of modified NFW profiles. We also estimate the dark matter annihilation rate  $\langle\sigma v\rangle$  required for each model.

The gamma-ray intensity in a given direction is the line-of sight integral of the dark matter number density,

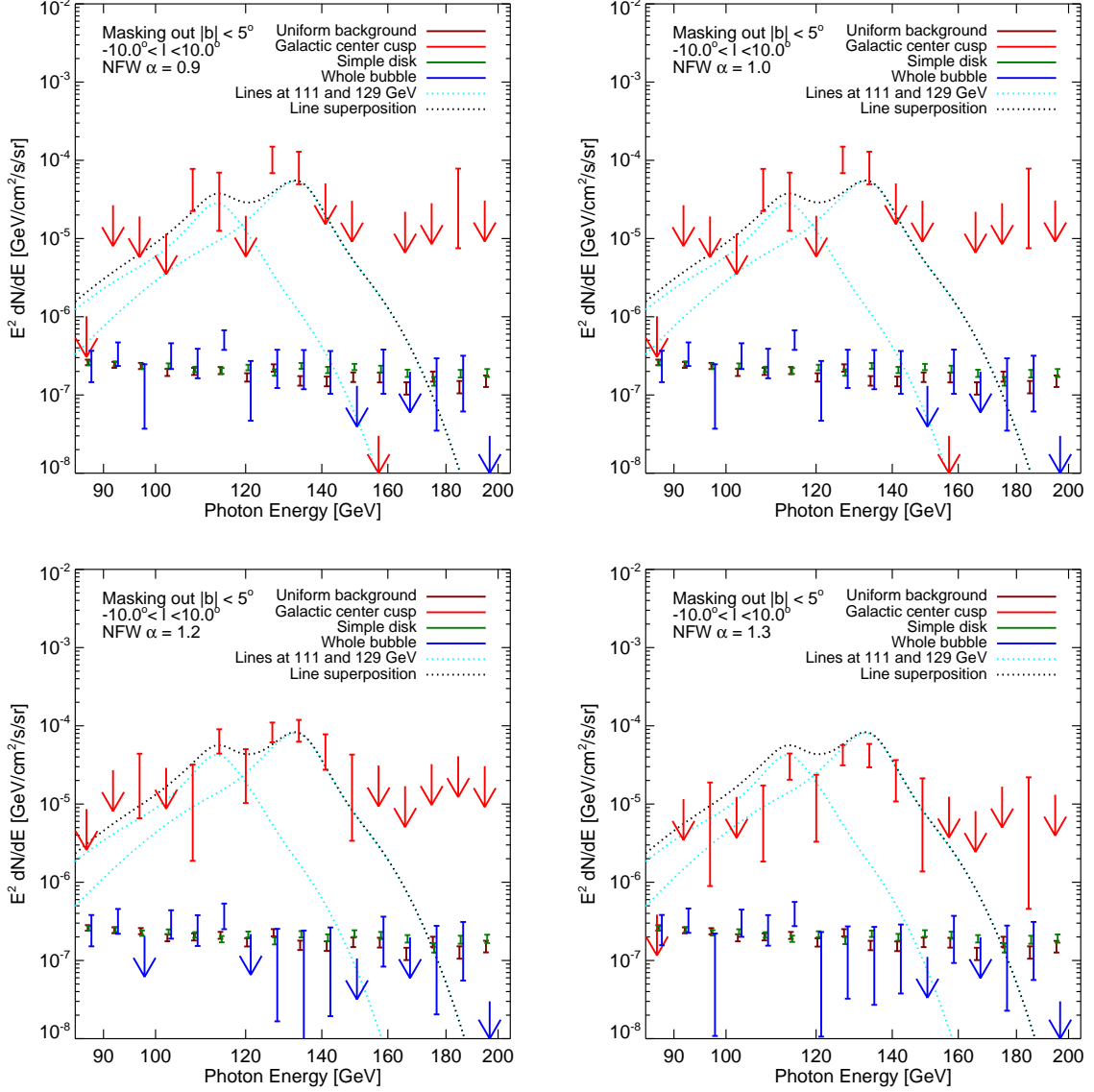


FIG. 22.— Same as right panel of Figure 10 but using modified NFW profiles with inner power law index  $\alpha$  for the DM density. The density is squared and projected along the line of sight to produce the cusp template for, from upper left to bottom right,  $\alpha = 0.9, 1.0, 1.2$ , and  $1.3$ , respectively. The fit prefers  $\alpha = 1.2$ , yielding a  $6.5\sigma$  significance by combining the central 7 bins with  $> 1\sigma$  each.

squared, along a given direction,

$$\frac{d\Phi_\gamma}{dE_\gamma} = \frac{1}{8\pi} \frac{\langle\sigma v\rangle_{\gamma\gamma}}{m_\chi^2} 2\delta(E - E_\gamma) r_\odot \rho_\odot^2 J, \quad (2)$$

with:

$$J = \int_{\text{cusp}} db \int_{\text{cusp}} dl \int_{\text{l.o.s.}} \frac{ds}{R_\odot} \cos b \left( \frac{\rho(r)}{\rho_\odot} \right)^2, \quad (3)$$

where the integral is over the cusp structure,  $\langle\sigma v\rangle_{\gamma\gamma}$  is the partial annihilation cross-section for  $\chi\chi \rightarrow \gamma\gamma$ ,  $m_\chi$  is the WIMP mass ( $E_\gamma = m_\chi$ ),  $R_\odot \simeq 8.5$  kpc is the distance from the Sun to the GC (Ghez et al. 2008),  $\rho(r)$  is the WIMP halo profile,  $\rho_\odot \simeq 0.3$  GeV cm $^{-3}$  is the often-used WIMP density at the Solar system (Jungman et al. 1996),  $r = (s^2 + R_\odot^2 - 2sR_\odot \cos \ell \cos b)^{1/2}$  is the Galactocentric distance and  $s$  is the line of sight distance. We use  $\rho_\odot \simeq 0.3$  GeV cm $^{-3}$  to facilitate comparison with

earlier work, but a higher value  $\rho_\odot \simeq 0.4$  GeV cm $^{-3}$  (Catena & Ullio 2009) would reduce our  $\langle\sigma v\rangle$  values by a factor of 1.7.

For halo profiles  $\rho(r)$ , we consider the Navarro-Frenk-White (NFW) profile (Navarro et al. 1996),

$$\rho_{\text{NFW}}(r) = \frac{\rho_s}{(r/r_s)^\alpha (1 + r/r_s)^{3-\alpha}} \quad (4)$$

with  $r_s = 20$  kpc. The value of  $\rho_s$  is determined by requiring  $\rho(r_\odot) = 0.3$  GeV cm $^{-3}$ . In Figure 22, we show the energy spectrum of the cusp structure using the NFW profile with various values of  $\alpha$ . Interestingly, we obtain a  $6.5\sigma$  ( $5.6/5.9\sigma$  for one/two line case after trials factor correction) detection of the cusp assuming  $\alpha = 1.2$ . This corresponds to a  $p$  value  $10^4$  times smaller than  $5\sigma$ .

We also consider the case of the Einasto profile,

$$\rho_{\text{Einasto}}(r) = \rho_s \exp\left\{-\frac{2}{\alpha E} \left[ \left( \frac{r}{r_s} \right)^{\alpha E} - 1 \right] \right\} \quad (5)$$

Models	Before trials	After trials (one line)	Trials factor (one line)
Gaussian (centered)	$5.0\sigma$	$3.7\sigma$	300
Gaussian (off center, $\theta > 40^\circ$ )	$5.5\sigma$	$3.7\sigma$	6000
unbinned $\ell$	$5.2\sigma$	$3.2\sigma$	6000
unbinned $\ell$ ( $\theta > 40^\circ$ )	$4.9\sigma$	$2.8\sigma$	6000
unbinned $b$	$4.8\sigma$	$3.5\sigma$	300
unbinned $b$ ( $\theta > 40^\circ$ )	$4.6\sigma$	$3.2\sigma$	300
NFW $\alpha = 1.0$ (off center)	$6.1\sigma$	$4.5\sigma$	6000
NFW $\alpha = 1.2$ (off center)	$6.5\sigma$	$5.0\sigma$	6000
NFW $\alpha = 1.3$ (off center)	$6.0\sigma$	$4.4\sigma$	6000
NFW $\alpha = 1.4$ (off center)	$5.6\sigma$	$3.8\sigma$	6000
NFW $\alpha = 1.5$ (off center)	$5.2\sigma$	$3.2\sigma$	6000
<b>Einasto (off center)</b>	<b><math>6.6\sigma</math></b>	<b><math>5.1\sigma</math></b>	<b>6000</b>

TABLE 2

THE DETECTION SIGNIFICANCE OF THE GAMMA-RAY CUSP FOR VARIOUS MODELS. SEE §4.2 FOR A DISCUSSION OF TRIALS FACTORS.

Models	After trials (two line)	Trials factor (two line)
Gaussian (centered)	$4.3\sigma$	36
Gaussian (off center, $\theta > 40^\circ$ )	$4.2\sigma$	720
NFW $\alpha = 1.0$ (off center)	$4.9\sigma$	720
NFW $\alpha = 1.2$ (off center)	$5.4\sigma$	720
NFW $\alpha = 1.3$ (off center)	$4.8\sigma$	720
NFW $\alpha = 1.4$ (off center)	$4.3\sigma$	720
NFW $\alpha = 1.5$ (off center)	$3.8\sigma$	720
<b>Einasto (off center)</b>	<b><math>5.5\sigma</math></b>	<b>720</b>

TABLE 3

THE DETECTION SIGNIFICANCE OF THE GAMMA-RAY CUSP STRUCTURE WITH DIFFERENT MODELS. SEE §4.2 FOR A DISCUSSION OF TRIALS FACTORS. MASKING OUT  $0.5^\circ$  AROUND THE GC AREA DOES NOT AFFECT THE RESULTS.

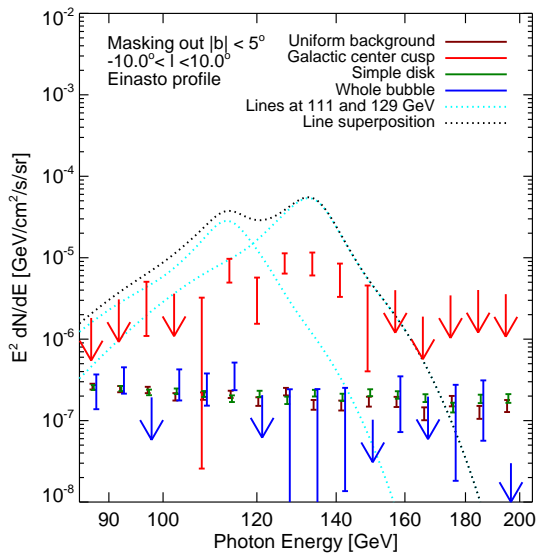


FIG. 23.— Same as right panel of Figure 10 but using an Einasto ( $\alpha = 0.17$ ) dark matter profile template to fit the data, we obtain a  $6.5\sigma$  detection of the cusp only using the central 7 bins with  $> 1\sigma$  each.

with  $r_s = 20$  kpc and  $\alpha = 0.17$  (Einasto 1965; Navarro et al. 2004). This template provides a slightly better fit, with  $6.6\sigma$  ( $5.7/6.0\sigma$  for one/two line case after trials factor correction) detection of the cusp. Table 2 and Table 3 lists the resulting significance for all the models.

## 8. HOW TO CONFIRM THIS SIGNAL QUICKLY: A MODIFIED SURVEY STRATEGY

The fact that high-incidence-angle photons are superior for line detection raises an exciting possibility: the scan strategy of *Fermi*-LAT could be altered for 1 year to confirm the 130 GeV line (if real) at  $5\sigma$  with no trials factor, a significance that would be widely regarded as a discovery. If more than one line is present, the additional data would help characterize it.

*Fermi* has usually scanned the sky in survey mode, observing the full sky every 2 orbits with occasional slews to targets of opportunity. This strategy is excellent for uniformity of full-sky coverage, but is far from optimal for collecting high-incidence-angle photons from the GC.

From the spacecraft data files for the first 3.7 years (through week 202), it is a straightforward exercise to derive the fraction of the time the GC is accessible. We impose the constraints that the roll angle be within  $35^\circ$  of zenith (as in standard survey mode) and that the GC have an incidence angle of  $45^\circ < \theta < 55^\circ$ . We consider only times when the spacecraft is not in the South Atlantic Anomaly (SAA) and the `DATA_QUAL` flag is good. These constraints allow the GC to be observed 40.6% of the time. This exceeds the exposure time of our ( $40^\circ < \theta < 60^\circ$ ) sample (observed 9.7% of the time) by more than a factor of 4. In other words, LAT could gather high  $\theta$  photons from the GC  $4\times$  faster than it usually does with a simple change to the observing strategy.



Because we wish to point  $\sim 50^\circ$  away from the GC anyway, it would still be possible to maintain coverage of the inner  $110^\circ$  radius about the GC. On the other half of the sky, survey mode would continue as usual. Although this change may be sub-optimal for some science projects, it would be a net benefit to the entire inner Galaxy, home to a great many scientific objectives.

We believe the trade would be worth it. After 1 year of altered observing, we would have a sample of high incidence photons equal to the current sample, and could evaluate their significance directly, in the absence of any trials factor. In addition to confirming the line at 130 GeV, other lines (113 GeV) may also become significant with additional data. At this point in the LAT mission, there are few ways for the instrument to dramatically improve its sensitivity to new physics in its remaining lifetime. This is a golden opportunity.

## 9. DISCUSSION AND CONCLUSION

*Morphology:* Using 3.7 years of *Fermi*-LAT data, we have identified a resolved gamma-ray cusp structure toward the Galactic center region. To reveal this structure in a simple, model-independent way, we first take a linear combination of smoothed maps that cancels out continuum emission in the plane and inspect the residual. We find that this structure only appears in the energy range from  $\sim 120$  GeV to  $\sim 140$  GeV after searching  $80 < E < 200$  GeV maps (Figures 3-5, and 19). The FWHM of the cusp morphology, if modeled with a Gaussian, is  $\lesssim 4^\circ$  and is unrelated to the *Fermi* bubble structure (as suggested by Profumo & Linden 2012). No other region of the sky reveals any significant excess in this energy range.

*Template regression:* We perform a Poisson likelihood analysis to obtain the energy spectrum of the gamma-ray cusp. We create maps in energy bins 5.5% wide, and model each map as a linear combination of templates including the cusp template, a uniform gamma-ray background, a thin gamma-ray disk tracing the Galactic plane, and the *Fermi* bubble structure. By modeling the data with a linear combination of templates and maximizing the Poisson likelihood of observing the observed counts, we are able to separate the cusp emission from the *Fermi* bubbles and the Galactic disk. To the extent that the template is actually correct, this “matched filter” gives an optimal estimate of the flux in each energy bin. The uncertainty estimates include marginalizing over the uncertainty in the other templates coefficients. We do not make *a priori* assumptions about the dark matter profile. For a template centered on the GC, we find that the cusp emits gamma rays with a luminosity of  $(3.2 \pm 0.6) \times 10^{35}$  erg/s, or  $(1.7 \pm 0.4) \times 10^{36}$  photons/sec. The null hypothesis of zero intensity is ruled out by  $5.0\sigma$  ( $3.7\sigma$  with trials factor).

Motivated by the apparent offset between the cusp and the GC, we repeat the template fit with a cusp template

centered at  $(\ell, b) = (-1.5, 0)$  (Figure 17), with the local significance rising to  $5.5\sigma$ , but with a larger trials factor, diluting the global significance.

*Line profile:* The energy spectrum of the cusp structure at  $E \gtrsim 80$  GeV is consistent with a single spectral line (at energy  $127.0 \pm 2.0$  GeV with  $\chi^2 = 4.48$  for 4 d.o.f.) convolved by the LAT energy response (Rajaraman et al. 2012). A pair of lines at  $110.8 \pm 4.4$  GeV and  $128.8 \pm 2.7$  GeV provides a marginally better fit (with  $\chi^2 = 1.25$  for 2 d.o.f.). These line energies suggest a WIMP annihilating to  $\gamma\gamma$  and  $\gamma Z$ . Fitting the two lines jointly, we find a WIMP mass of  $127.3 \pm 2.7$  GeV with  $\chi^2 = 1.67$  for 3 degrees of freedom. The line pair is also compatible with a 141 GeV WIMP annihilating through  $\gamma Z$  and  $\gamma h$  for  $m_h \sim 125$  GeV, as in the “Higgs in Space” scenario (Jackson et al. 2010). We note that the uncertainty of overall absolute energy scale of LAT is  $[-10, +5]\%$  (Fermi-LAT Collaboration 2012).

*Interpretation as dark matter:* Given the properties of the gamma-ray cusp, and assuming it originates from dark matter annihilation, constraints on the dark matter density profile and annihilation rate or cross section can be placed on various models (e.g. Goodman et al. 2011; Jackson et al. 2010; Cline 2012; Bertone et al. 2009; Dudas et al. 2012; Geringer-Sameth & Koushiappas 2012). At present, the extrapolation from the local dark matter density into the Galactic center is uncertain enough that there are large uncertainties in the cross section. We do not attempt to improve those estimates in this work.

*Comparison to previous work:* The recent study by The Fermi-LAT collaboration: M. Ackermann et al. (2012) put constraints on line emission from the inner Galaxy, excluding photons within  $|b| < 5^\circ$ . Therefore, their constraints are not in conflict with the signal claimed in this paper, which is mostly within  $5^\circ$  of the GC. Ackermann et al. searched for dark matter gamma-ray line signal from 4.8 GeV to 264 GeV (Fermi-LAT Collaboration: M. Ackermann et al. 2012), updating the results from the earlier study with 11 months *Fermi*-LAT data (Abdo et al. 2010). The results from this study are obtained from two years of *Fermi*-LAT data and used the Pass 6 processing, which has somewhat worse background and instrumental systematics compared to Pass 7.

The Galactic center is known to be a region with diffuse high energy gamma-ray emission (Aharonian et al. 2006a), especially the Galactic center ridge (Aharonian et al. 2006b). High energy gamma rays are produced by cosmic rays interacting with interstellar gas or giant molecular clouds in the central  $\sim 200$  parsecs. We note that the resolved cusp is incompatible with a point source given that it extends to  $\sim 4^\circ$ . To check for contribution from unresolved point sources, we have repeated our analyses masking

out regions with  $|b| < 1^\circ$ , and have obtained similar results, confirming that the cusp is not associated with the Galactic ridge.

*The future:* The next version of *Fermi*-LAT data (Pass 8) will move us closer to realizing the full scientific potential of the LAT (Atwood 2012). The expected improvements include reduced backgrounds, increased effective area, reduced point-spread function, better understanding of the systematic uncertainties, and particularly extending the energy reach to higher photon energy. Finally, the calorimeters of LAT have been demonstrated to effectively operate as a standalone instrument providing imaging of the sky at  $E \gtrsim 10$  GeV, albeit with worse image resolution (at the level of  $1^\circ$ ) with a large potential increase in the effective area at high energy and large angle (Atwood 2012). Such data would be valuable for future studies of the gamma ray line(s).

*A modified survey strategy:* As discussed in section 8, the LAT could acquire significance on spectral line emission from the Galactic center 4 times as fast as it currently does with a change in observing strategy. In other words, a single year of observing the GC 40% of the time would yield more significance on these gamma-ray lines than all data currently in hand. A factor of 2 improvement would come from observing the GC more often, and another factor of 2 by maintaining a high incidence angle ( $45^\circ < \theta < 55^\circ$ ), yielding photon events with better energy reconstruction. We hope that the evidence presented in this paper for a signal in general, and specifically the superior value of the high- $\theta$  events can be used to justify such a change.

Data acquired from the new survey strategy, along with Pass 8 improvements, will be able to better constrain the morphology of the gamma-ray cusp and study in detail the line emission in  $110 \lesssim E \lesssim 140$  GeV, determine if there are two (or more) lines, and measure the ratios of the line strengths. Such measurements may be the key to differentiating between WIMP models and deepening our understanding of the dark sector.

*Is this a "discovery?":* The local (without trials factor) significance of our results is high:  $5.0\sigma$  for the cen-

tered Gaussian template fit to energy bins,  $5.25\sigma$  for the unbinned Gaussian fit at ( $\ell = -1.5, b = 0$ ), and  $6.5\sigma$  by fitting the NFW dark matter profile centered at  $(-1.5, 0)$  with power index  $\alpha = 1.2$ , with similar results for an Einasto profile. Given such high significances, it would be tempting to call this detection a "Discovery." However, we have a number of concerns:

- The cusp is off-center by  $1.5^\circ$  (200 pc) and this was not expected. If the theoretical prior against this is strong, then this reduces confidence in the result – or at least a WIMP-related interpretation of the result. It is now an urgent question for simulators and theorists to determine whether this offset is unlikely or not in a spiral Galaxy with a significant bar.
- The trials factor for this discovery is significant: The energy part is roughly 300 for a generic line search, though much less for the  $\gamma\gamma, \gamma Z$  scenario. The trials factor for the position offset could also be substantial.
- Now that we have characterized what looks like a robust signal, the path to a truly convincing discovery is clear: modify the survey strategy to accumulate signal on the GC as quickly as possible, and repeat the experiment with no trials factor.

**Acknowledgments:** We thank Neal Weiner, Tracy Slatyer, Christopher Stubbs, Lars Hernquist, and Michael Kuhlen for helpful discussions. We acknowledge the use of public data from the *Fermi* data archive at <http://fermi.gsfc.nasa.gov/ssc/>. This work would not be possible without the work of hundreds of people, over many years, to design, build, and operate *Fermi*. M.S. and D.P.F. are partially supported by the NASA Fermi Guest Investigator Program. This research made use of the NASA Astrophysics Data System (ADS) and the IDL Astronomy User's Library at Goddard (Available at <http://idlastro.gsfc.nasa.gov>).

## REFERENCES

- Abdo, A. A. et al. 2010, Phys. Rev. Lett., 104, 091302  
 Abramowski, A. et al. 2011, Physical Review Letters, 106, 161301, 1103.3266  
 Ackermann, M. et al. 2011, Physical Review Letters, 107, 241302, 1108.3546  
 Aharonian, F. et al. 2006a, Physical Review Letters, 97, 221102, arXiv:astro-ph/0610509  
 ——. 2006b, Nature, 439, 695, arXiv:astro-ph/0603021  
 Atwood, W. 2012, in American Astronomical Society Meeting Abstracts, Vol. 219, American Astronomical Society Meeting Abstracts, 145.18  
 Atwood, W. B. et al. 2009, ApJ, 697, 1071, 0902.1089  
 Bergström, L. 2000, Reports on Progress in Physics, 63, 793, arXiv:hep-ph/0002126  
 Bergström, L., & Ullio, P. 1997, Nuclear Physics B, 504, 27, arXiv:hep-ph/9706232  
 Bergström, L., Ullio, P., & Buckley, J. H. 1998, Astroparticle Physics, 9, 137, arXiv:astro-ph/9712318  
 Bertone, G., Hooper, D., & Silk, J. 2005, Phys. Rep., 405, 279, arXiv:hep-ph/0404175  
 Bertone, G., Jackson, C. B., Shaughnessy, G., Tait, T. M. P., & Vallinotto, A. 2009, Phys. Rev. D, 80, 023512, 0904.1442  
 Boyarsky, A., Malyshev, D., & Ruchayskiy, O. 2012, ArXiv e-prints, 1205.4700  
 Bringmann, T., Huang, X., Ibarra, A., Vogl, S., & Weniger, C. 2012, ArXiv e-prints, 1203.1312  
 Catena, R., & Ullio, P. 2009, 0907.0018  
 Cline, J. M. 2012, ArXiv e-prints, 1205.2688  
 Dobler, G., Finkbeiner, D. P., Cholis, I., Slatyer, T., & Weiner, N. 2010, ApJ, 717, 825, 0910.4583  
 Dudas, E., Mambriani, Y., Pokorski, S., & Romagnoni, A. 2012, ArXiv e-prints, 1205.1520  
 Edmonds, Y. V. 2011, PhD thesis, Stanford University  
 Einasto, J. 1965, Trudy Astrofizicheskogo Instituta Alma-Ata, 5, 87  
 Fermi-LAT Collaboration. 2012, ArXiv e-prints, 1206.1896

- Fermi-LAT Collaboration: M. Ackermann et al. 2012, ArXiv e-prints, 1205.2739
- Gehrels, N., & Michelson, P. 1999, *Astropart. Phys.*, 11, 277
- Geringer-Sameth, A., & Koushiappas, S. M. 2012, ArXiv e-prints, 1206.0796
- Ghez, A. M. et al. 2008, *ApJ*, 689, 1044, 0808.2870
- Gondolo, P., & Silk, J. 1999, *Physical Review Letters*, 83, 1719, arXiv:astro-ph/9906391
- Goodman, J., Ibe, M., Rajaraman, A., Shepherd, W., Tait, T. M. P., & Yu, H.-B. 2011, *Nuclear Physics B*, 844, 55, 1009.0008
- Hooper, D., & Profumo, S. 2007, *Phys. Rep.*, 453, 29, arXiv:hep-ph/0701197
- Jackson, C. B., Servant, G., Shaughnessy, G., Tait, T. M. P., & Taoso, M. 2010, *JCAP*, 4, 4, 0912.0004
- Jungman, G., Kamionkowski, M., & Griest, K. 1996, *Phys. Rept.*, 267, 195, hep-ph/9506380
- Mattox, J. R. et al. 1996, *ApJ*, 461, 396
- Navarro, J. F., Frenk, C. S., & White, S. D. M. 1996, *Astrophys. J.*, 462, 563, astro-ph/9508025
- Navarro, J. F. et al. 2004, *MNRAS*, 349, 1039, astro-ph/0311231
- Profumo, S., & Linden, T. 2012, ArXiv e-prints, 1204.6047
- Rajaraman, A., Tait, T. M. P., & Whiteson, D. 2012, ArXiv e-prints, 1205.4723
- Su, M., & Finkbeiner, D. P. 2012, ArXiv e-prints, 1205.5852
- Su, M., Slatyer, T. R., & Finkbeiner, D. P. 2010, *ApJ*, 724, 1044, 1005.5480
- Tempel, E., Hektor, A., & Raidal, M. 2012, ArXiv e-prints, 1205.1045
- The Fermi-LAT collaboration: M. Ackermann et al. 2012, ArXiv e-prints, 1205.6474
- Weiner, N., & Yavin, I. 2012, ArXiv e-prints, 1206.2910
- Weniger, C. 2012, ArXiv e-prints, 1204.2797